The 16th Symposium on Polar Science

2-5 December 2025

National Institute of Polar Research Research Organization of Information and Systems

Session OA

Antarctic Meteorites

Abstracts

Conveners: Akira Yamaguchi (NIPR)

Molybdenum isotopic composition in carbonaceous chondrite meteorites

<u>Tatsuki Takeya</u>¹, Tetsuya Yokoyama¹, Ikshu Gautam¹
(1 Institute of Science Tokyo, Earth and Planetary Sciences)

Abstract

Recent technical innovations in high-precision mass spectrometry have revealed that meteorites exhibit "nucleosynthetic isotope anomalies", representing differences in the stable isotope compositions of elements including Ti, Cr, Mo, Ru, and Nd compared to those of the Earth. One significant discovery is the "isotopic dichotomy", meaning that carbonaceous chondrite (CC) meteorites and non-carbonaceous (NC) meteorites have isotopic compositions different from each other. For example, in the ε⁵⁰Ti-ε⁵⁴Cr diagram, NC and CC meteorites are plotted in distinct locations, a phenomenon that cannot be explained by simple two-component mixing^[1]. Isotopic dichotomy also exists for Mo, with NC and CC meteorites plotted on separate regression lines (NC- and CC-lines) in the μ^{95} Mo- μ^{94} Mo diagram^[2]. The existence of such isotopic dichotomy suggests that the source materials of NC and CC were spatially and temporally separated in the early solar system. In particular, the source materials of CC contain more neutron-rich nuclides than those of NC. On the other hand, the Mo isotopic composition of the Earth's mantle (BSE) lies between the NC- and CC-lines and does not match any known meteorite^[3]. Previous studies have reported isotopic compositional similarities between Earth and enstatite chondrites (EC) for many elements (e.g., O, Ca, Cr, and Ti)^[4]. However, the Mo isotopic composition of EC is deficient in s-process nuclides compared to the Earth^[5]. Therefore, in addition to EC-like primordial material, s-process-rich material may have contributed to the formation of the Earth with regard to Mo^[6].

To further investigate the relationship between the Mo isotope dichotomy and the dynamics of Earth's formation, we measured the Mo isotope compositions of six meteorites obtained from the National Institute of Polar Research: Y-980115 (CI1), A-881595 (CR2), Y-791717 (CO3), Y82102 (CK5), A-881902 (Acapulcoite), and Y-981725 (Lodranite). The samples were digested using HF, HNO₃, and HCl, followed by chemical separation of Mo using anion exchange resins. The Mo isotopic composition was measured using N-TIMS. We found that Y-980115 exhibited the most sprocess-rich isotopic composition among CC meteorites reported to date. This isotopic anomaly is closer to the Mo isotopic composition of BSE than to that of CC meteorites previously reported, and is considered to constrain the Mo isotopic composition of CC-like material that may have caused the Moon-forming giant impact.

References: [1] Warren, P. H., 2011, EPSL 311, 93. [2] Budde, G. et al., 2016, EPSL 454, 293. [3] Budde, G. et al., 2019, Nat. Astron. 3, 736-741. [4] Dauphas, N. 2017, Nature 541, 521. [5] Render, J. et al., 2017, GPL 3, 170. [6] Yokoyama, T. et al., 2019 ApJ 883, 62.

Small-scale geochemical variations in CI chondrites and CI-like materials

<u>Karina López García¹</u>, Tetsuya Yokoyama¹, Nao Nakanishi², Ikshu Gautam¹

¹Department of Earth and Planetary Sciences, Institute of Science Tokyo

²Department of Earth Sciences, Waseda University

Carbonaceous chondrites are among the most valuable materials for investigating the early Solar System, as their geochemical differences reflect variations in the conditions during planetary formation and evolution [1-3]. Within this group, CI chondrites are regarded as some of the most primitive Solar System materials, with bulk chemical compositions that closely match the solar photosphere for most elements [1,2]. The unofficially named Yamato-type (CY) chondrites are ungrouped carbonaceous chondrites that exhibit mineralogical, chemical, and isotopic characteristics intermediate between CI and CM chondrites. However, their parent bodies appear to have experienced both aqueous alteration and thermal metamorohism [3-5].

To trace intrinsic chemical and isotopic heterogeneity within carbonaceous parent bodies, arising both from inherited variations during the formation of their building blocks and from secondary planetary processes, small-scale elemental abundance variations, together with isotope anomalies, such as those of Cr, have proven to be valuable tools [6-9]. Therefore, this study aims to investigate the small-scale chemical variability and nucleosynthentic Cr isotope anomalies in various carbonaceous materials, such as CI chondrites and CI-like materials, to gain better insights into the formation and evolutionary histories of their parent bodies.

Particle samples with masses between 1 to 5 mg of two CI chondrites (Orgueil and Ivuna), one CY1 chondrite (Y-980115) and three CY2 (Y-86789, Y-86720 and B-7904) were digested with a mixture of acids (HF, HNO3 and HCl) and heated at high temperature (~220 °C). The digested samples were dissolved in 0.5 M HNO3, from which a 10% aliquot was split off for the determination of the abundances of 54 elements using a triple-quadrupole ICP-MS instrument (iCAP TQ, Thermo Sci), while the remaining solution was used for Cr separation through a three-step column chemistry procedure combining an extraction chromarographic resin (DGA normal, Eichron), as well as anion and cation exchange resins, followed by Cr isotope ratio measurements using a TIMS instrument (Triton Plus, Thermo Sci).

The elemental abundance ranges observed in both CI and CY samples vary by more than 20% relative to the average CI composition for several elements (Figure 1). Among CI chondrites, Orgueil samples exhibit greater heterogeneity for most elements, particularly Na, P, Ca, Mn, Cu, Zn, Sr, Ba, and rare-earth elements (REEs), whereas Ivuna samples show abundances closer to the mean CI values. Similarly, the CY1 sample Y-980115 shows less variation and abundances closer to the average CI composition than the three CY2 chondrites, which display wider abundance ranges for most elements, as well as enrichments in refractory elements, such as Ca, Fe, Ni, Zr, and REEs. While chemical heterogeneity within CI and CY chondrites can be attributed to secondary planetary processes, the differences between Y-980115 and the rest of the CY chondrites may also stem from fractionation during the formation of their parent bodies.

The samples exhibit variable values of both ϵ^{53} Cr, ranging from 0.09 ± 0.03 to 0.43 ± 0.03 , and ϵ^{54} Cr, ranging from 0.28 ± 0.06 to 2.51 ± 0.05 . The ϵ^{53} Cr and ϵ^{54} Cr values of most samples are consistent with those previously reported in the literature [6,7,9], except for one Orgueil sample, which shows a particularly low ϵ^{54} Cr value (0.28 ± 0.06), as well as one B-7904 sample with a lower ϵ^{54} Cr value (0.72 ± 0.05) compared to the rest of the CY chondrites, and one Y-86720 sample with a significantly elevated ϵ^{54} Cr value (2.48 ± 0.05). This variation likely reflects both the presence of coexisting 54 Cr-rich/ 53 Cr-poor and 54 Cr-poor/ 53 Cr-rich carrier phases, along with the contribution from 53 Mn decay [e.g., 6, 7].

References

[1] Morlok A. et al. 2006. Geochim. Cosmochim. Acta 70. [2] Barrat J. A. et al. 2012. Geochim. Cosmochim. Acta 83. [3] Ebihara et al. 2025. Geochim. Cosmochim. Acta 389. [4] King A. J. et al. 2019 Geochemistry 79.4. [5] Suttle et al. 2023 Geochim. Cosmochim. Acta 361. [6] Yokoyama et al. 2023. Sci. Adv. 9(45). [7] Qin et al. 2010. Geochim. Cosmochim. Acta

74. [8] Zhu et al. 2021. Geochim. Cosmochim. Acta 301. [8] Petitat et al. 2011. Astrophys. J. 736:23. [9] Zhu et al. 2025. Astrophys. J. Lett. 984:L54.

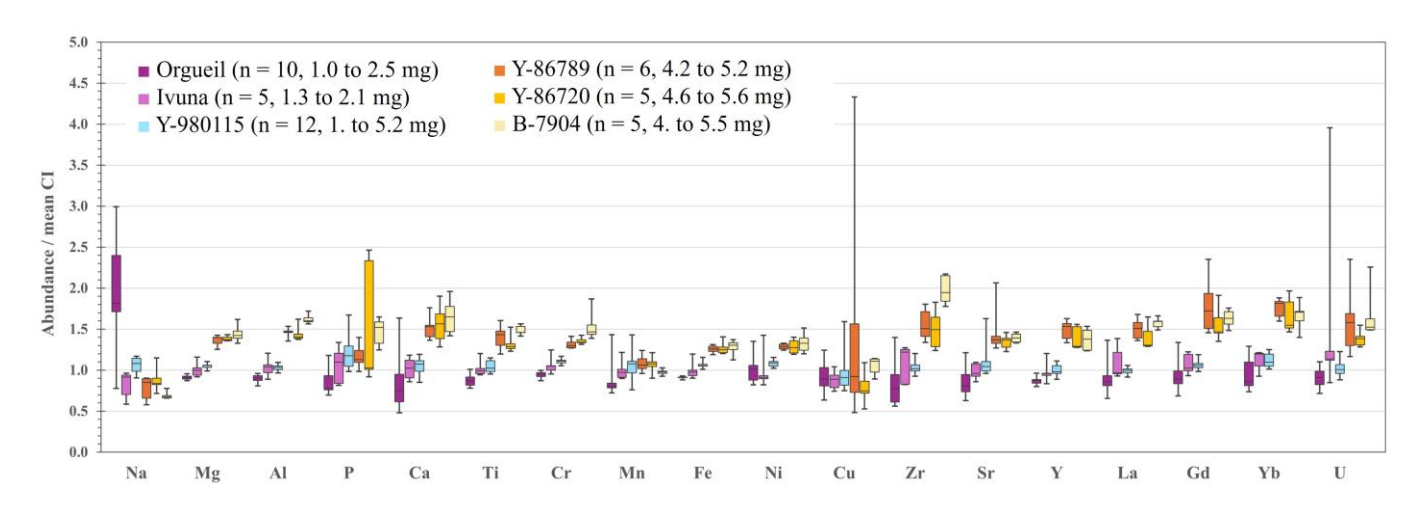


Figure 1. Elemental abundances ranges of Orgueil, Ivuna, Y-980115, Y-86789, Y-86720, and B-7904. Data normalized to mean CI-values.

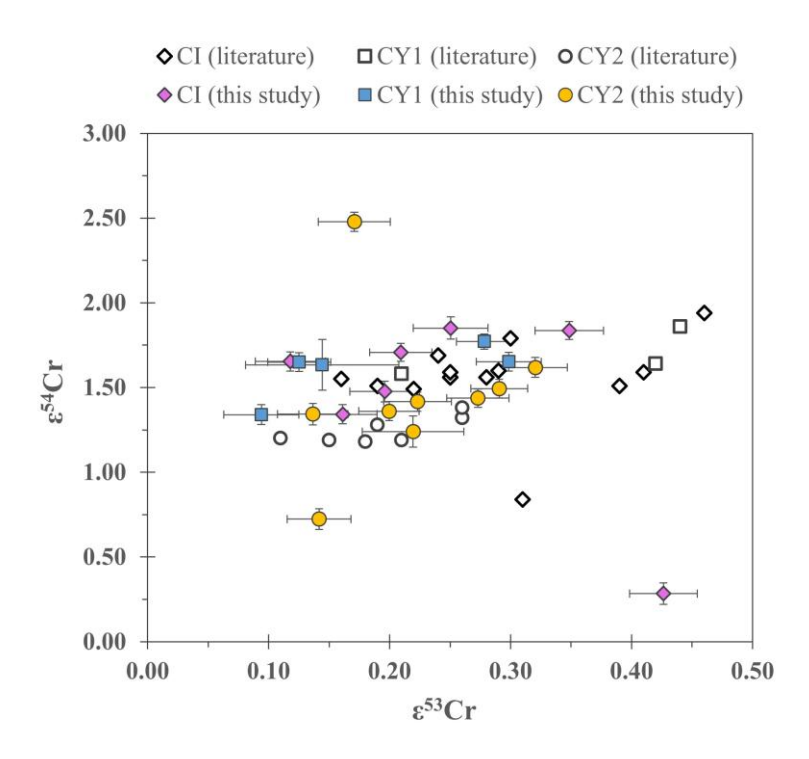


Figure 2. ε^{54} Cr versus ε^{53} Cr diagram for CI and CY chondrites. Literature data from [6] and those compile in [8].

Formation and evolution of the CY chondrite parent body

Yuto Takaki¹, Masaaki Miyahara¹, Akira Yamaguchi², and Naotaka Tomioka³

¹Hiroshima University, ²National Institute of Polar Research, ³Kochi Institute for Core Sample Research,

Japan Agency for Marine-Earth Science and Technology,

The CY chondrites exhibit similar petrological and chemical characteristics between the most primitive CI and CM chondrites (Ikeda, 1992). They show the closest spectral match to materials on the surface of asteroid Ryugu, from which the Hayabusa2 mission returned samples (King et al., 2019). Ryugu is a rubble-pile asteroid formed through repeated collisional events, and recent studies have reported multiple shock-related textures such as microfaults and slickenside in its returned grains (Tomioka et al., 2023; Miyahara et al., 2024). Zolensky et al. (2022) reported the presence of glassy material ("agglutinate") formed by melting of regolith in the Orgueil CI chondrite. Until recently, CI chondrites and Ryugu grains were generally regarded as largely unshocked, primitive materials. However, the discoveries of shock-related textures in both Ryugu particles and CI chondrites suggest otherwise, representing a significant departure from the conventional understanding.

An important feature of CY chondrites is that they experienced thermal metamorphism after aqueous alteration. Previous studies suggest this heating event was extremely short in duration, ranging from several years to mere hours, and was caused by impact events as heat sources (King et al., 2019). These imply that impacts played a crucial role in the formation and evolution of the CY chondrite parent body. Studies on shock metamorphism in CY chondrites are still limited, but this process plays a crucial role in the disruption and thermal evolution of planetary bodies of hydrated chondrites. The aim of this study is to elucidate the formation and evolutionary history of CY chondrites through detailed petrographic analysis of shock-related textures.

We analyzed nine CY chondrites: Yamato (Y)-980115, Y-86029, Y-86737, Y-980134, Y-980115 (124A), Y-86720, Y-86789, Y-82162, Belgica (B)-7904, and two CY-like CM chondrites: Y-791198 and Asuka (A)-881655. Microtextural observations were conducted using a field emission scanning electron microscope (FE-SEM). Subsequently, quantitative analyses of chemical compositions were carried out using an electron probe microanalyzer (EPMA).

FE-SEM observations revealed the coexistence of three distinct textural domains within the same specimen: (1) regions that show little to no evidence of shock metamorphism, (2) "agglutinates" that appear to have formed through shockinduced melting, and (3) regions characterized by abundant subparallel cracks. Agglutinate consists of normally zoned euhedral olivine crystals, Fe-Ni sulfide spherules, vesicle, and mesostasis glass. Agglutinates and subparallel cracks were identified in four and two samples, respectively, and both features were observed in Y-980115 and Y-980134, which exhibit brecciation. However, regions showing distinct shock metamorphic textures were not observed in many samples, the fraction of the regions exhibiting developed subparallel cracks does not exceed ~2% of the total, and the abundance of agglutinates is limited to ~0.3%. The brecciated CY chondrite Y 980115 contains several clasts whose chemical compositions and mineral assemblages differ

markedly from those of the majority of fragments, indicating significant heterogeneity within the host rock.

Shock recovery experiments using CI/CY chondrites (Nakahashi et al., 2025) showed that subparallel fracturing and the onset of melting become prominent at around 4 GPa and 10 GPa, respectively. Whether the subparallel cracks and agglutinates observed in the investigated CY chondrite are equivalent to those identified in shock-recovery experiments is still under consideration. However, if these features were formed through shock metamorphism, this would suggest that fragments which have experienced different shock pressures can coexist within a single meteorite. These observations suggest that CY

chondrites were fragmented by past impact events, and that fragments with different shock histories were subsequently reassembled to form the present-day rock. Although the origin of clasts within the Y 980115 CY chondrite remains unresolved, the clasts display chemical compositions and mineral assemblages distinct from the surrounding fragments. These features may strongly suggest either intrinsic heterogeneity within the CY chondrite parent body or material mixing resulting from an impact with another body of different origin. Such observations provide critical insights not only into the formation history of the CY parent body but also into the role of impacts in reshaping and evolving its internal structure.

References

- King A.J., H.C. Bates, D. Krietsch, H. Busemann, P.L. Clay, P.F. Schofield, S.S. Russell, (2019) The Yamato-type (CY) carbonaceous chondrite group: Analogues for the surface of asteroid Ryugu? Geochemistry, 79: 125531
- Miyahara M., Noguchi T., Matsumoto T., Tomioka N., Miyake A., Igami Y., Seto Y., Haruta M., Saito H., Hata S., Ishii H. A., Bradley J. P., Ohtaki K. K., Dobrică E., Leroux H., Le Guillou C., Jacob D., de la Peña F., Laforet S., Mouloud B.-E., Marinova M., Langenhorst F., Harries D., Beck P., Phan T. H. V., Rebois R., Abreu N. M., Gray J., Zega T., Zanetta P.-M., Thompson M. S., Stroud R., Burgess K., Cymes B. A., Bridges J. C., Hicks L., Lee M. R., Daly L., Bland P. A., Zolensky M. E., Frank D. R., Martinez J., Tsuchiyama A., Yasutake M., Matsuno J., Okumura S., Mitsukawa I., Uesugi K., Uesugi M., Takeuchi A., Sun M., Enju S., Takigawa A., Michikami T., Nakamura T., Matsumoto M., Nakauchi Y., Abe M., Nakazawa S., Okada T., Saiki T., Tanaka S., Terui F., Yoshikawa M., Miyazaki A., Nakato A., Nishimura M., Usui T., Yada T., Yurimoto H., Nagashima K., Kawasaki N., Sakamotoa N., Okazaki R., Yabuta H., Naraoka H., Sakamoto K., Tachibana S., Watanabe S., and Tsuda Y. (2024) Microscopic slickenside as a record of weak shock metamorphism in the surface layer of asteroid Ryugu. Meteoritics & Planetary Science 59: 3181–3192.
- Nakahashi T., Miyahara M., Yamaguchi A., Kobayashi T., Yusa H., Miyakawa M., Tomioka N., Takaki Y, Noguchi T., Matsumoto T., Miyake A., Igami Y, Seto Y. (2025) Experimental constraints on the shock history of CI chondrites and Ryugu grains, Earth and Planetary Science Letters, 668, 119559.
- Suttle M.D., King A.J., Harrison C.S., Chan Q.H.S., Greshake A., Bartoschewitz R., Tomkins A.G., Salge T., Schofield P.F., Russell S.S., (2023) The mineralogy and alteration history of the Yamato-type (CY) carbonaceous chondrites. Geochimica et Cosmochimica Acta, 361: 245-264
- Tomioka N., Yamaguchi A., Ito M., Uesugi M., Imae N., Shirai N., Ohigashi T., Kimura M., Liu M.-C., Greenwood R. C., Uesugi K., Nakato A., Yogata K., Yuzawa H., Kodama Y., Hirahara K., Sakurai I., Okada I., Karouji Y., Okazaki K., Kurosawa K., Noguchi T., Miyake A., Miyahara M., Seto Y., Matsumoto T., Igami Y., Nakazawa S., Okada T., Saiki T., Tanaka S., Terui F., Yoshikawa M., Miyazaki A., Nishimura M., Yada T., Abe M., Usui T., Watanabe S., Tsuda Y. (2023) A history of mild shocks experienced by the regolith particles on hydrated asteroid Ryugu. Nature Astronomy, 7, 669–677.
- Zolensky M., Mikouchi T., Hagiya K., Ohsumi K., Komatsu M., Cheng A., Le L., (2022) Evidence for impact shock and regolith transportation on CM, CI, and CV chondrite parent asteroids. Meteorics & Planetary Science 57; 1902-1923

Chemical characterization of secondary minerals in CY chondrite Y 980115

Ryoga Maeda¹, Thibaut Van Acker², Rei Kanemaru³, Frank Vanhaecke², Akira Yamaguchi⁴ and Steven Goderis⁵

¹Submarine Resources Research Center (SRRC), Japan Agency for Marine-Earth Science and Technology (JAMSTEC), Japan

²Atomic & Mass Spectrometry Research Unit, Ghent University, Belgium

³Institute of Space and Astronautical Science, Japan Aerospace Exploration Agency (JAXA), Japan

⁴National Institute of Polar Research (NIPR), Japan

⁵Archaeology, Environmental changes, and Geo-Chemistry (AMGC), Vrije Universiteit Brussel, Belgium

Introduction

Since meteorites recovered from Antarctica constitute by number more than 60% of the meteorite population, the Antarctic meteorite collection continues to play a pivotal role in cosmochemistry. This collection includes many rare types of meteorites, including not only lunar and martian meteorites but also meteorites found only in Antarctica. For example, the relatively new carbonaceous group, the Yamato-type (CY) is only found in Antarctica and composed of more than 10 meteorites [1-3]. According to previous studies on CY chondrites [1, 2], these meteorites underwent aqueous alteration on the parent bodies to varying extents and also late-stage thermal metamorphism at peak temperatures > 500 °C. The mineralogical, textural, and chemical features of these meteorites are often intermediate between CI and CM chondrites and a recent study has suggested that CY chondrites can be classified into two groups: CI-like CY chondrite (CYi) and CM-like CY chondrites (CYm) [3]. Yamato (Y) 980115 has a relatively large recovered mass of ~772 g and was initially classified as a CI chondrite. However, based on prior studies, Y 980115 can be re-classified as a CY chondrite, belonging to the CYi group. In a framework of a series of recent studies, we aim to better understand the comprehensive elemental behaviors during aqueous alteration on the parent bodies. For this purpose, a set of CI and CM samples, including a Ryugu particle, were examined for their elemental distributions among the constituent minerals, focusing in particular on trace elements [4, 5]. Y 980115 is included in this work as CY chondrites might genetically relate to CI, CM, or even asteroid Ryugu. Moreover, CY chondrites are documented to contain minerals that are rare or absent in other carbonaceous chondrites, such as periclase and rhodochrosite. Some of these minerals likely formed during post-heating event(s) and as such record the effect of such event(s) on the elemental redistribution [6].

Experimental

Polished thick sections (PTSs) were prepared for Y 980115 as well as for three CI chondrites (Ivuna, Orgueil, and Oued Chebeika 002). Firstly, back-scattered electron (BSE) images and the X-ray maps of the major elements for the PTSs were obtained using a field emission (FE)-EPMA at JAXA, Japan. Once their constituent minerals were roughly identified based on the major element maps and BSE images obtained, FE-EPMA analysis was performed at JAXA to determine the major element abundances in each constituent mineral. Parallel to the EPMA analysis, the areas of interest on each PTS were defined for subsequent LA-ICP-TOF-MS mapping. Finally, quantitative element mapping was conducted using LA-ICP-TOF-MS at Ghent University, Belgium [7].

Results and Discussion

Based on the preliminary results, Y 980115 is dominated by a phyllosilicate matrix with abundant Fe-sulfides and magnetite, which is consistent with previous studies [2]. Clasts enriched in Mg, Fe, and Mn are also present in the matrix (Fig. 1), which can be identified as FeO-bearing periclase (MgO) or magnesiowüstite ((Mg, Fe)O) based on previous studies. However, while King *et al.* (2019) reported that only a few grains of Ca-carbonates were observed in Y 980115 [2], our sample displays relatively abundant Ca-carbonates (~5 vol.%), which are all Mg, Fe, Mn-bearing. On the other hand, Urashima *et al.* (2025) identified 60 and 3 grains of carbonates found in Y 980115 as nesquehonite (Mg(HCO₃)(OH)·2H₂O) and calcite, respectively [8]. In terms of phosphates, at least two grains of Na-Mg-Fe phosphate were found in Y 980115, which has not previously been reported, although Yui *et al.* (2025) identified three grains of Mg-phosphate [9]. Interestingly, most of the phosphates found in this study and King *et al.* (2019) are apatite, while Yui *et al.* (2025) did not find any apatite. This variation of lithology among the different sections of Y 980115 suggest that these secondary minerals are heterogeneously distributed in the meteorite, which is also the case for Ryugu particles [10]. Carbonates and Ca-phosphates are also found in the CI chondrites analyzed in this study. However, no Mg, Fe, Mn-clasts or Ca-poor phosphates are present in them, indicating that Y 980115 has a distinct mineralogy from CI chondrites.

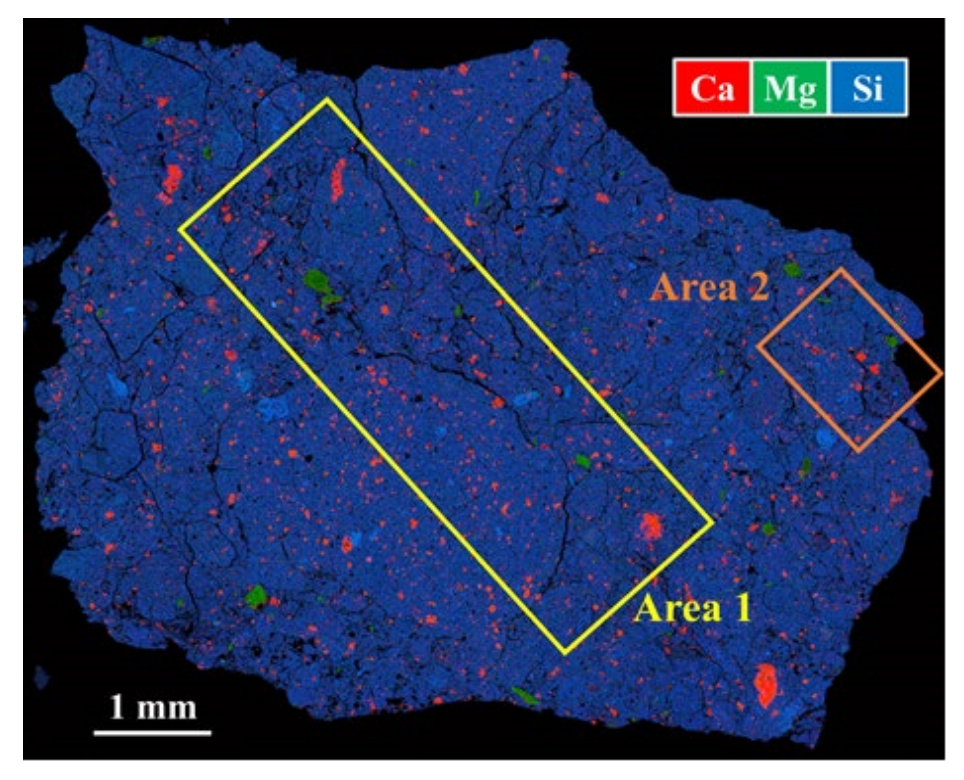


Fig. 1. A combined RGB X-ray elemental map of Y 98011 with red: Ca, green: Mg, and blue: Si. The areas analyzed using LA-ICPTOF-MS are indicated by the yellow and orange rectangles as Area 1 and Area 2, respectively.

According to LA-ICP-TOF-MS mapping, Sr and Ba, which are usually regarded fluid mobile elements, are concentrated in the Ca-carbonates of Y 980115 (Figs. 1 and 2). Some of the Ca-carbonates contain a moderate amount of rare earth elements (REEs), but this is not the case for all the grains. REEs are more abundant in Ca-phosphates than in Ca-carbonates, which is consistent with their partition coefficients [11]. A similar distribution of REEs is observed for the CI chondrites. In contrast, Mg, Fe, Mn-clasts and Na-Mg-Fe phosphates, ofrmed in a late dtage due to the post-heating event(s), contain almost none of such elements [2, 8]. As such, these minerals could be indicators of the effect of heating on the elemental re-distribution [6]. At the scale of the studied sample, the formation of these secondary minerals might have a negligible effect on the trace element distribution. Given the heterogeneous distribution of the secondary minerals in Y 980115, however, any effects of these secondary minerals of the elemental budget may be highly localized. Future work on more primitive carbonaceous chondrites and Ryugu particles will confirm the heterogeneous distribution of comparable mineral phases.

References

[1] Ikeda Y. (1992) Proc. NIPR Symp. Antarct. Meteorites **5**, 49-73. [2] King A. J. et al. (2019) Geochim. **79**, 125531. [3] Ebihara M. et al. (2025) Geochim. Cosmochim. Acta **389**, 200-210. [4] Maeda R. et al. (2024) MetSoc 2024, #6274 (abstract). [5] Maeda R. et al. (2025) Hayabusa Symp. 2025 (abstract) [6] Iizuka T. et al. (2025) Nature. [7] Maeda R. et al. (2023) J. Anal. At. Spectrom. **38**, 369-381. [8] Urashima S. et al. (2025) Anal. Sci. **41**, 689-695. [9] Yui H. et al. (2025) Anal. Sci. **41**, 323-328. [10] Yamaguchi A. et al. (2023) Nat. Astron. **7**, 398-405. [11] Green T. H. (1994) Chem. Geo. **117**, 1-36.

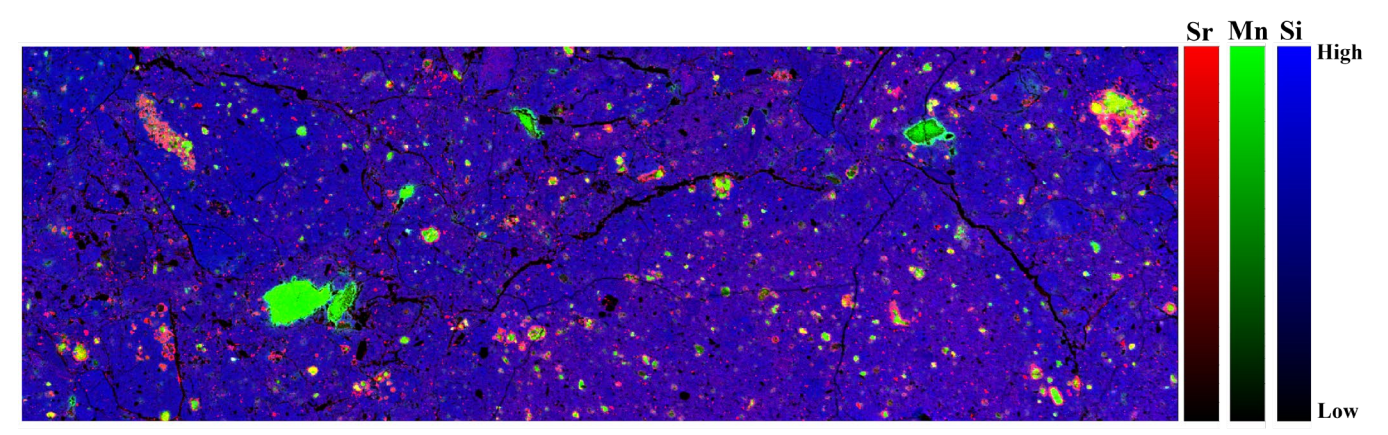


Fig. 2. A combined RGB elemental map of Area 1 obtained using LA-ICP-TOF-MS with red: Sr, green: Mn, and blue: Si.

Hydrogen content in CI, CY and CM chondrites

M. Ebihara¹, M. A. Islam¹, Naoki Shirai², Aiko Nakato³, Akira Yamaguchi³ and Takahito Osawa⁴ ¹ Tokyo Metropolitan Uniersity, ²Kanagawa University, ³NIPR and ⁴Japan Atomic Energy Agency

Introduction

The hydrogen content of a meteorite is often indirectly determined from the water content, which is often determined gravimetrically as part of wet analysis. The neutron-induced prompt gamma-ray analysis (PGA) method is a method for directly determining the hydrogen content. The Antarctic CY and CM chondrites were analyzed using PGA, and the contents of major elements, including hydrogen, were reported at the NIPR Antarctic Meteorite Symposiums in 2023 and 2024, respectively. In this study, we report the hydrogen contents of three non-Antarctic CI chondrite meteorites. We also compare and discuss the hydrogen contents of CI, CY, and CM chondrites.

Experimental

PGA was carried out using the JRR-3 research reactor of the Japan Atomic Energy Agency. The three non-Antarctic CI chondrites, Orgueil, Ivuna and Alais, along with three CY (Y 980115, B-7904 and Y-86720) and one CM (Y-793321), were newly analyzed by PGA in this study. Powder/chip sample of each meteorite with a mass of about 117-266 mg, with the exception of Alais (25.7 mg), was used. In this study, the powder sample was heated at 110 °C in an oven and cooled at room temperature in a desiccator. A cycle of heating and cooling was repeated several times until the mass of the sample became constant.

Results and Discussion

Water contained in rock samples can be classified into adsorbed water, absorbed water, interlayer water, crystal water, structural water, etc. CI, CY, CM and CR chondrites contain more than 1 wt% water. When these meteorite samples are heated, the water corresponding to each state of existence is released stepwise in the order described above. In this study, the mass losses of Orgueil, Ivuna, and Alais were measured when they were brought to constant mass at 110°C, and losses of 7.24, 5.88 and 4.10 wt%, respectively, were observed. The hydrogen contents of the meteorites measured by PGA were 2.07, 2.01 and 1.67 wt%, which correspond to 18.6, 18.1, and 15.0 wt% water. Therefore, 38, 32 and 27% of the water was lost during heating of the samples. The water lost at constant mass is thought to be due to the contribution of interlayer water in addition to adsorbed and absorbed water. CI chondrites contain layered silicate minerals such as serpentine and saponite, and it is thought that the water molecules held between the layers escaped when heated. The water content of the Orgueil meteorite was reported to be 9.06 wt% several weeks after its fall [1]. The difference between this and the value in this study (18.6 wt%; converted value) is mainly due to the atmospheric water molecules being absorbed between the layers of the layered silicate as interlayer water after the fall, and it is thought that the amount of acquired water molecules has now reached saturation. In this context, what significance does the hydrogen content of CI chondrites obtained in this study have?

Many CY and CM chondrites are known to have undergone aqueous alteration, followed by thermal metamorphism on their parent bodies. The hydrous minerals in CY and CM were formed by aqueous alteration processes on the parent body, and the adsorbed, absorbed and interlayer water was probably lost due to subsequent heating events and the environment in space. However, minerals derived from aqueous alteration containing crystal water and hydroxyl groups must have survived, and therefore, the crystal and structural water are thought to have been preserved. So, did the water content change after falling on Antarctica? Since a positive correlation was observed between the hydrogen and chlorine contents of CY chondrites (Ebihara et al., 2025), we are forced to assume not only that there have been no significant changes since their fall onto Antarctica, but that they retain the composition they had at the time of the parent body's formation. It is suggested that aqueous alteration occurred in a closed system, with only minor contributions from adsorbed, absorbed and interlayer water. The correlation between hydrogen and chlorine as seen in CY was not observed in CM chondrites, suggesting that aqueous alteration and subsequent thermal alteration occurred locally on the CM parent body. This indicates that the formation of parent bodies and subsequent metamorphic processes were significantly different between the CY and CM chondrites.

References

[1] Cloez S, Compt. R Acad. Sci. Paris, 58, 986-988, 1864. [2] Ebihara, M. et al., Geochim. Cosmochim. Acta, 389, 200-210, 2025.

Mineralogy, geochemistry and reflectance spectra of Jikharra 001, a eucrite melt breccia

A. Y. C. Wong¹, B. G. Rider-Stokes¹, L. F. White¹, S. L. Jackson¹, R. C. Greenwood¹, M. Anand¹, M. M. Grady¹

School of Physical Sciences, The Open University, Milton Keynes, MK7 6AA, UK.

Introduction: The Howardite-Eucrite-Diogenite (HED) meteorites are believed to have originated from the asteroid (4) Vesta, a large (diameter ~525 km) asteroid situated in the main belt [1]. However, it has been suggested that some of them, in particular those that have anomalous geochemical and isotopic compositions, may have been contaminated with exogenous material during impact events, or even originate from different asteroidal bodies [2,3]. Furthermore, data returned from the DAWN mission suggest a potential lack of magma ocean or complete differentiation of Vesta [4]. Jikharra 001 is a eucrite melt breccia, and the distinct lithic and melt lithologies in this sample present a valuable opportunity to understand the chemical and isotopic effects of impact on a eucritic sample. This report presents preliminary results from a study of the mineralogy, geochemistry, and the UV-Vis-NIR spectroscopic features of Jikharra 001.

Sample and methods: A large fragment of Jikharra 001 (110g) was obtained from a meteorite collector. The fragment was cut and made into a polished thick section. The polished thick section was subsequently coated in carbon (5 nm) and investigated using a TESCAN CLARA SEM (beam current 1 nA, accelerating voltage 20 kV) at The Open University (OU), UK. High-resolution backscatter electron (BSE) and energy dispersive X-ray spectroscopy (EDS) maps of the sample were obtained. Chemical compositions were determined using an electron probe microanalyser (EPMA: CAMECA SX100, beam current 20 nA, accelerating voltage 15 kV), also located at the OU. A small portion (~1g) of material was broken off from the main mass and crushed by hand using an agate mortar and pestle, to produce a homogenised powder with grain sizes of >=50 μm. Subsequently, the UV-Vis-NIR spectrum of the sample was measured using a JASCO MSV-5700 UV-Vis-NIR microspectrophotometer (MSP), with a magnification of 16x and an aperture of 400 μm, following established procedures [5]. Oxygen isotope analysis is planned in the near future and will be carried out following established procedures [6, 7]. All analyses described were carried out at the OU.

Results and discussion: Jikharra 001 consists of two distinct lithologies, one that represents recrystallised melt, and the other that represents residual lithic material. The melt region is mainly composed of pyroxene grains, surrounded by a recrystallised "matrix" that is compositionally related to pyroxene and plagioclase (Fig. 1a). The residual lithology consists mainly of coarse-grained pyroxene and interstitial plagioclase, most of which have a lath-like shape (Fig. 1b). Pyroxenes in both lithologies exhibit augite exsolution lamellae of varying thickness ($10\sim50~\mu m$). A more detailed description of the lithologies present in Jikharra 001 can be found in [8].

Surprisingly, the mineralogy of the recrystallised melt region is very similar to that of the residual lithology. The chemical composition of pyroxene and plagioclase within each region only shows a small degree of variability, and notably, no significant distinction can be made across the two lithologies. The pyroxene in the melt region is Fe-rich (En_{35,4-37,4}Fs_{56,8-60,8}Wo_{2,4-7,8}), with an Mg# = 37.0-39.3, and Fe/Mn = 33.9-35.5 (n=9); the plagioclase has an average composition of An₉₀ (n=3). The pyroxene in the residual region is similarly Fe-rich ($E_{135,4-36.6}F_{558,2-61.1}W_{02,7-6.1}$), with an Mg# = 37.6-38.0, and Fe/Mn = 31.9-36.3 (n=5); and the plagioclase also has an average composition of An₉₀ (n=4). This may suggest that the melt region contain only a small amount of melt, largely preserving the chemistry of the original lithology despite having underwent melting and recrystallisation. The presence of exsolution textures in pyroxene found in both regions may also suggest that those in the recrystallised melt region could be clasts broken off from the original lithology. In addition, the close similarity of the geochemistry of the pyroxene and plagioclase present in Jikharra 001 with that of the main HED suite supports a strong link between them. Furthermore, the geochemistry of Jikharra 001 lies almost completely within the basaltic eucrite area (Figs. 2 a,b,c). We therefore propose that the protolith of Jikharra 001 was of a basaltic eucrite composition, which again implies that the impact event had not significantly altered the major mineralogical composition of Jikharra 001. However, it is currently not known whether the impact event resulted in trace element or oxygen isotope contamination; further analysis is planned, which will provide more insights into this. The oxygen isotope composition of the two distinct lithologies will be analysed shortly, and results will be reported at the time of the Symposium. This will help constrain the parent body of Jikharra 001, specifically whether it is likely to have originated from the asteroid (4) Vesta, believed to be the parent body of the main HED suite, or if it has an alternative V-type origin, i.e. from a V-type asteroid outside the dynamical orbit of Vesta.

We also compared the UV-Vis-NIR spectrum of Jikharra 001 to that of other HEDs and V-type asteroids, following band structure analysis methods outlined in [5]. In general, the spectrum of Jikharra 001 is typical of V-type asteroids [9], which supports a relationship with V-types and (4) Vesta. However, both the band I centre (BIc) and band II centre (BIIc) of Jikharra 001 notably deviate from the database of V-type asteroids, as well as that of other HED samples analysed, shifting longward. This shift may be attributed to the chemistry of pyroxene present in Jikharra 001, for example, due to it being more ferroan [10].

Summary: Jikharra 001 is a eucrite melt breccia with a geochemistry that suggests a strong affinity to basaltic eucrites, and we propose that its protolith is of a basaltic eucrite composition. However, it also has spectral features that differ from other HEDs. Further work planned for the near future will help constrain its origins. It is expected that these results will provide further insights into the significance and effects of impact events on the chemical and isotopic composition of HED meteorites.

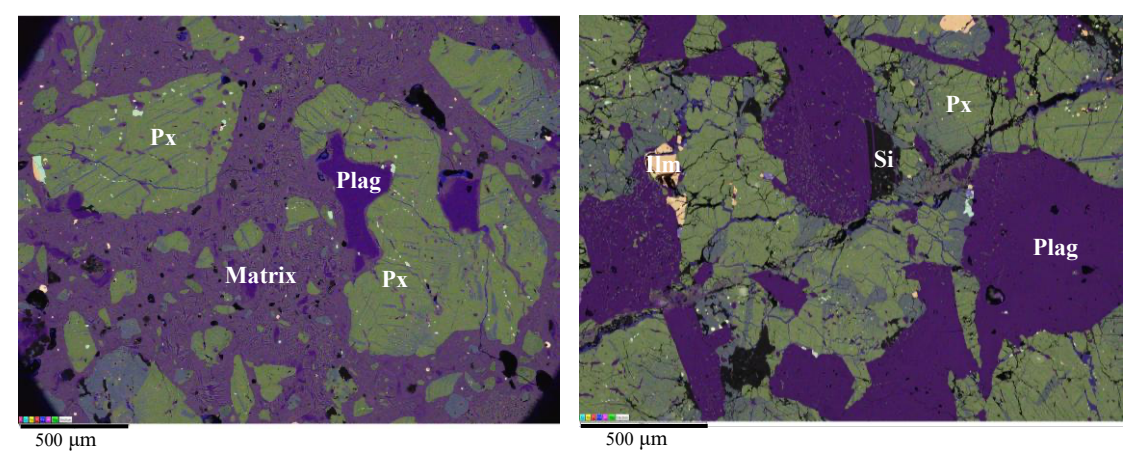


Figure 1. False-colour EDS maps showing two distinct lithologies in Jikharra 001. Left: recrystallised melt; right: residual lithology.

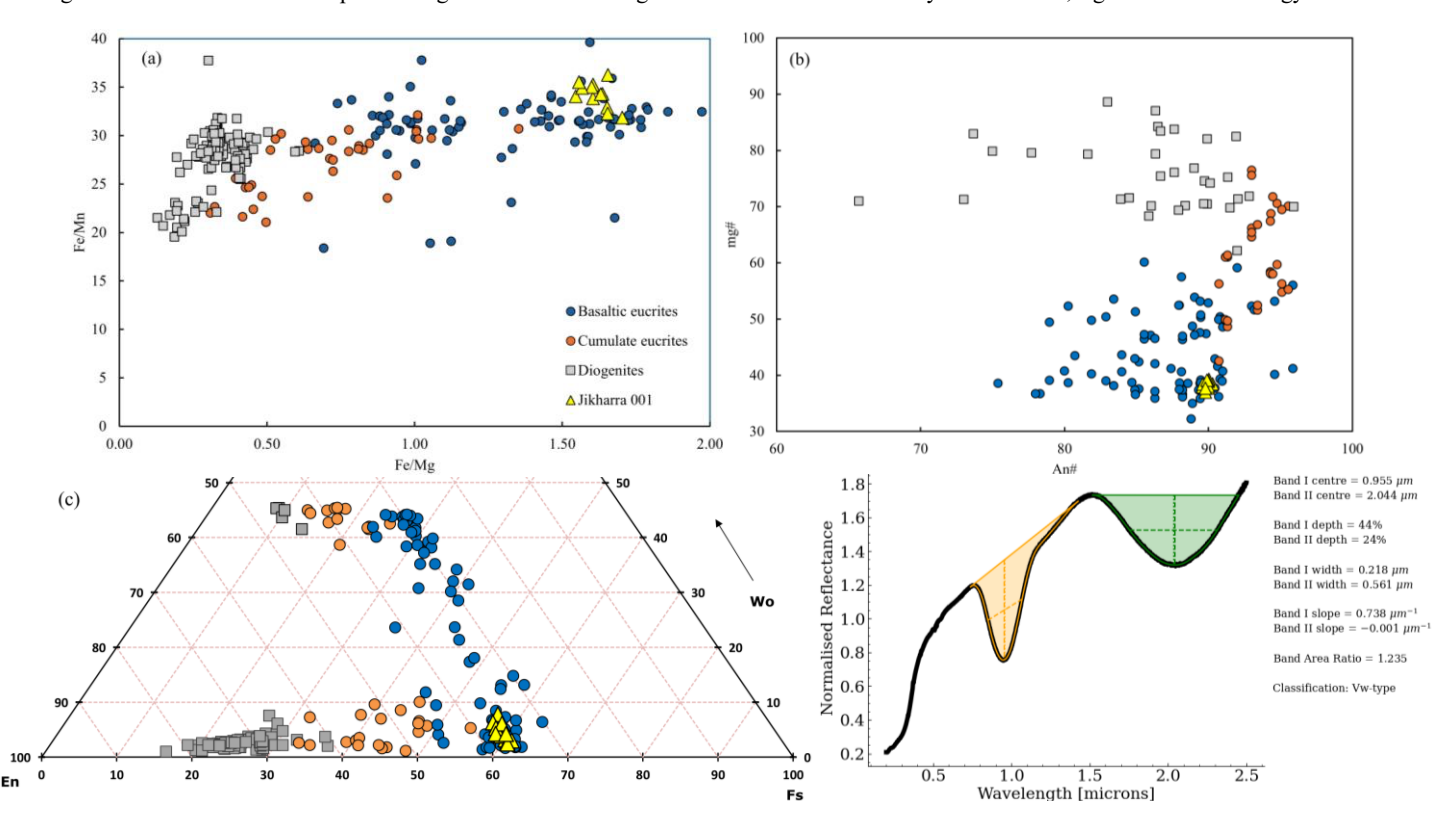


Figure 2. Mineral composition of major phases in Jikharra 001, compared to other HEDs (data from [1]). Bottom right: UV-Vis-NIR spectra.

References: [1] Mittlefehldt, D.W. (2015). *Geochemistry*, 75(2), pp.155–183. [2] Janots, E. et al. (2012). *MAPS*, 47(10), pp.1558–1574. [3] Zhang, C. et al. (2019). *Planetary and Space Science*, 168, pp.83–94. [4] McSween, H.Y. et al. (2019). *Geochemistry*, 79(4), pp.125526. [5] Rider-Stokes, B.G. et al. (2025). *Icarus*, 432, p.116506. [6] Miller, M.F. (2002). *Geochim. Cosmochim. Acta*, 66(11), pp.1881–1889. [7] Greenwood, R.C. et al. (2017). *Geochemistry*, 77(1), pp.1–43. [8] Wang, Z. et al. (2023). *54th LPSC*, Abstract #2806. [9] DeMeo, F.E. et al. (2009). *Icarus*, 202(1), pp.160–180. [10] Klima, R.L. et al. (2011). *MAPS*, 46(3), pp.379–395.

Cathodoluminescence mineralogy of silica minerals in eucrites

Rei Kanemaru¹, Akira Yamaguchi², and Naoya Imae²

¹Institute of Space and Astronautical Science (ISAS), Japan Aerospace Exploration Agency (JAXA),

² National Institute of Polar Research

Silica minerals are among the most commonrock-forming minerals on Earth, exhibiting various polymorphs under different temperature and pressure conditions. Therefore, understanding the characteristics of silica minerals is crucial for elucidating the thermal and shock history of the rocks. Recently, the combined method of Cathodoluminescence and Raman techniques has enabled detailed observation of the two-dimensional distribution of silica polymorphs (Fig. 1) [2, 3]. In this study, we employed this approach to conduct a systematic observation of silica minerals in eucrite meteorites.

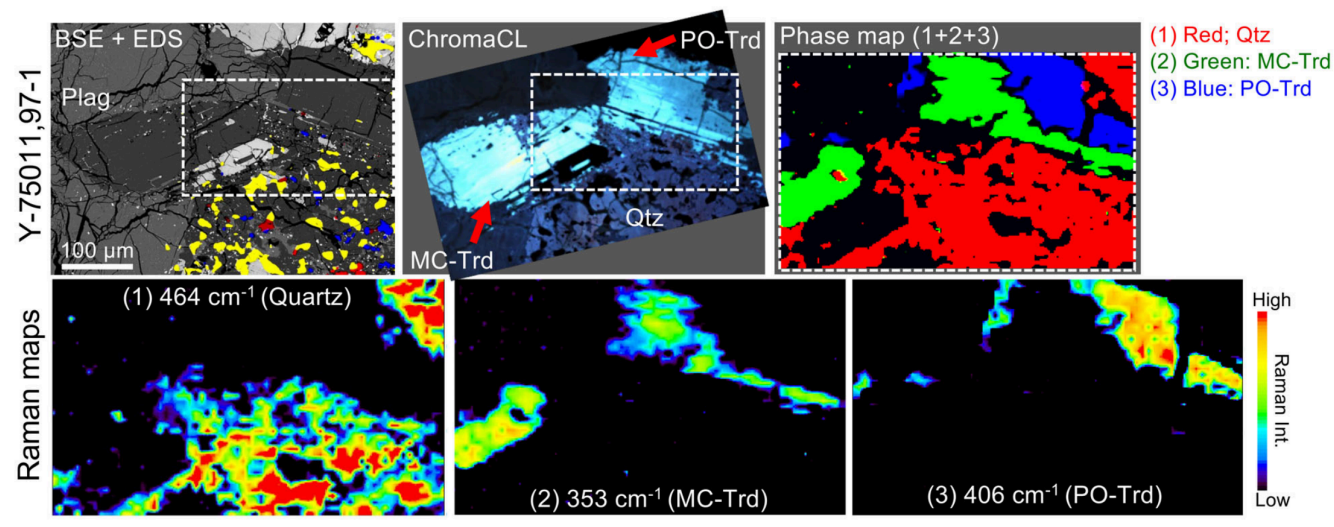


Fig. 1. Raman spectra and mapping of silica minerals in eucrite (modified Kanemaru et al., [1]).

We studied 13 basaltic eucrites and 4 cumulate eucrites, including nine Antarctic meteorites: Asuka (A) -881747, A-87272, Yamato (Y)-75011, Y-790266, Y-791195, Y-792510, Y 983366, Y 980433 and Elephant Moraine (EET) 90020, and eight non-Antarctic meteorites: Northwest Africa (NWA) 5356, NWA 7188, Agoult, Cachari, Moama, Moore County, Millbillillie, and Stannern. Samples of Antarctic meteorites were obtained from National Institute of Polar Research, Tokyo (NIPR) and NASA/Johnson Space Center (JSC), and those of non-Antarctic meteorites were obtained from meteorite dealers. An optical microscope, in Via Raman microscope (Renishow), a field emission scanning electron microscope (FE-SEM: JEOL JSM-7100) equipped with an energy dispersive spectrometer (EDS: Oxford AZtec Energy) and a color-cathodoluminescence imaging system (ChromaCL2: GATAN) at NIPR were used in this study. Chemical compositions were obtained using an electron probe microanalyzer (EPMA: JEOL JXA-8200) at NIPR and a field-emission electron probe microanalyzer (FE-EPMA: JEOL JXA-iHP200f) at ISAS/JAXA.

Silica minerals in eucrites exhibit various combinations, and their proportions change continuously [1, 4]. In this study, based on these variations, the eucrites were divided into four "Si-groups" according to their dominant silica phase: Si-0 (cristobalite-dominant eucrites), Si-I (quartz-dominant eucrites), Si-II (quartz and tridymite-dominant eucrites), and Si-III (tridymite-dominant eucrites) [1]. This paper presents a model that explains the formation pathways of silica minerals in eucrites and accounts for the distinct formation histories represented by each Si-group: tridymite crystallizes from alkali-rich immiscible melts (starting at $\geq \sim 1060^{\circ}$ C), cristobalite crystallizes from quenched melts ($\sim 1060^{\circ}$ C), and quartz crystallizes from extremely differentiated melts and/or by solid-state transformation from tridymite and cristobalite through interactions with sulfur-rich vapor below $\sim 1025^{\circ}$ C (for details, see the original paper). On the other hand, silica minerals in eucrites have also experienced various degrees of shock

metamorphism. The shock degreess of eucrites are classified from A (unshoked) to E (highly-shocked) based on the mineralogical characteristics of pyroxene and plagioclase (i.e., maskelynitization) [3]. In this study, as evidence of shock metamorphism other than high-pressure minerals, we found that silica glass (probably diaplectic glass) and MX tridymite, coexistence with MC tridymite in shock degree D and E eucrites. Thus, the presence of MX tridymite with silica glass implies that the MX tridymite corresponds to the transition phase that occurred during the conversion from MC tridymite into silica glass by modelate to higly shock metamorphism [2, 5]. Thus, silica minerals in eucrites can be used as key indicators for deciphering the detailed metamorphic history of eucrites.

References

[1] Kanemaru, R, et al. The nature and formation of silica minerals in eucrite meteorites: Insight into the protoplanetary magma crystallization. *Meteoritics & Planetary Science* (2025).

(https://doi.org/10.1111/maps.70045). [2] Kanemaru, R, et al. Experimental evidence of phase transition of silica polymorphs in basaltic eucrites: implications for thermal history of protoplanetary crust. *Scientific Reports* 14.1 (2024): 26414. (https://doi.org/10.1038/s41598-024-77544-x). [3] Kanemaru, R, et al. Estimation of shock degrees of eucrites using X-ray diffraction and petrographic methods. *Polar Science* 26 (2020): 100605.

(https://doi.org/10.1016/j.polar.2020.100605). [4] Ono, H, et al., Association of silica phases as geothermobarometer for eucrites: Implication for two-stage thermal metamorphism in the eucritic crust.. *Meteoritics & Planetary Science* 56, 6 (2021). (https://doi.org/10.1111/maps.13664). [5] Kanemaru, R, et al. Silica minerals in eucrites: Implication for crystallization and metamorphic history of Vestan crust. JPGU, abst. (2024).

Constrains on the Internal Structure and Evolution Timescale of Asteroid 4 Vesta Based on ϵ^{142} Nd- ϵ^{143} Nd Distribution Inferred from Magma Ocean Crystallization Model

S. Yamazaki¹, T. Mikouchi^{1,2} and A. Yamaguchi³

¹Dept. Earth and Planet. Sci., University of Tokyo, Hongo, Tokyo 113-0033, Japan (yamazaki-sojiro@g.ecc.u-tokyo.ac.jp)

²University Museum, University of Tokyo, Hongo, Tokyo 113-0033, Japan

³National Institute of Polar Research (NIPR), Tachikawa, Tokyo 190-0014, Japan

Introduction: Asteroid 4 Vesta is thought to have experienced a global magma ocean (VMO) during its early formation stage [1], and HED meteorites (howardites, eucrites and diogenites) are regarded as samples derived from its crust and perhaps upper mantle. Petrological studies suggest that the mineralogical and geochemical variations in HED meteorites may have originated from such a VMO [2]. In recent years, high-precision Nd isotopic data (ϵ^{142} Nd and ϵ^{143} Nd) have been reported for samples from differentiated planetary bodies such as Earth, Moon and Mars. Because Nd isotopic ratios are not significantly affected by secondary physical or chemical processes, they preserve robust records of source materials and provide valuable insights into early differentiation processes. For Mars and other bodies, ϵ^{142} Nd- ϵ^{143} Nd isotopic system have been widely used to estimate differentiation timescales and constrain magma ocean solidification [3]. However, no comparable application has yet been systematically made to Vesta, despite the availability of extensive HED samples. It therefore remains unresolved how the observed ϵ Nd values correspond to Vesta's internal stratification, source depths, and differentiation history from ϵ^{142} Nd- ϵ^{143} Nd isotopic sistem. This study addresses this gap by applying a VMO crystallization model to estimate the internal distributions of ϵ^{142} Nd and ϵ^{143} Nd within Vesta. By integrating the Sm-Nd decay systems into the crystallization framework, we place quantitative constraints on Vesta's internal structure and evolutionary timescales. Ultimately, this approach tests whether methods applied to other differentiated bodies can be extended to Vesta or not [4], offering new insights into the formation and geochemical evolution of one of the Solar System's earliest planetary building blocks.

Analytical methods: We estimated the distribution of Nd isotopic ratios in the Vesta formed during the VMO solidification using a model that incorporates fractional crystallization and the decay systems of ¹⁴⁶Sm-¹⁴²Nd and ¹⁴⁷Sm-¹⁴³Nd.

$$\begin{array}{lcl} N_{^{146,147}\mathrm{Sm}}(t) & = & N_{0^{146,147}\mathrm{Sm}}\mathrm{e}^{-\lambda_{146,147}\mathrm{Sm}t} \\ N_{^{142,143}\mathrm{Nd}}(t) & = & N_{0^{142,143}\mathrm{Nd}}\mathrm{e}^{-\lambda_{142,143}\mathrm{Nd}t} - \frac{dN_{^{146,147}\mathrm{Sm}}}{dt}\Delta t \\ \varepsilon_{^{142,143}\mathrm{Nd}} & \equiv & \left(\frac{\left(^{142,143}\mathrm{Nd}/^{144}\mathrm{Nd}\right)}{\left(^{142,143}\mathrm{Nd}/^{144}\mathrm{Nd}\right)_{\mathrm{std}}} - 1\right) \times 10^{4} \end{array}$$

In our calculations, the magma ocean was divided into depth-dependent layers, with 10^4 grids representing the vertical structure. Each layer was assumed to solidify from the bottm of the VMO at the core-mantle boundry to the surface. The Nd isotopic concentrations in the liquid phase and each solidified layer were calculated sequentially using batch crystallization model which combined the effects of Sm decay as the liquid fraction decreased from F = 1 to 0.

$$C_L = \frac{C_0}{D + F - DF}$$
, $C_S = \frac{DC_0}{D + F - DF}$, $D = \sum_i n_i D_i$

Here, C_L denotes the concentration of ^{146,147}Sm or ^{142,143}Nd isotopes in the liquid phase of the VMO, C_S is the concentration in the solid layer crystallized from the VMO, n_i represents the modal abundance of mineral spicies i and D_i represents the partition coefficient for mineral species i. This approach provided a detailed distribution of ε^{142} Nd and ε^{143} Nd in the Vesta. The mineral composition of the Vesta at various depths was estimated from the mineral composition of HED meteorites (Table 1). Partition coefficients for each mineral were derived from previous studies. Other parameters used in the calculations are summarized in Table 2. For the bulk Sm and Nd isotopic ratios of Vesta, we assumed values equivalent to those of CI chondrites [8-12].

Results and Discussion: The timing of Vesta's core formation t_1 is estimated to have occurred at approximately 1 Myr after the formation of calcium–aluminum-rich inclusions (CAI), in good agreement with previous geochronological studies [5]. This early differentiation age is geophysically and cosmochemically plausible, because the formation of a global magma ocean must have taken place while sufficient amounts of the short-lived radionuclide 26 Al (half-life \sim 0.7 Myr) were still present to provide the necessary internal heating. The inferred age of core segregation is therefore consistent with theoretical expectations for early-formed differentiated planetesimals. The timescale for the VMO crystallization τ is also estimated to have been on the order of \sim 1 Myr, again consistent with earlier thermal and petrological models [6]. Such a rapid solidification history reflects both the relatively small size of Vesta and the efficient cooling of its magma ocean, in contrast to the longer

crystallization intervals inferred for larger bodies such as the Mars or Moon. Furthermore, a previous work suggested that cumulate eucrites—thought to represent early crystallization products of the VMO—were buried to depths of roughly ~10 km beneath the surface [7]. The estimated crystallization depth of cumulate eucrites is the same as the source depth of cumulate eucrites inferred from our model, suggesting that they may have solidified directly from the VMO [2]. Our model additionally provides depth constraints for the other source materials of HED meteorites: basaltic eucrites are inferred to have originated from the source material which located at shallow levels near ~1 km depth and diogenites source material located at greater depths of ~15-60 km. It should be emphasized that the Nd isotopic composition infeerd from our model record the characteristics of source materials at specific depths within Vesta, rather than the crystallization sites of the present-day meteorites [15]. The observed HED lithologies were formed from partial melts extracted from these source regions and solidified as eucrites and diogenites. Subsequently, howardites were produced through brecciation of these lithologies by impact processes [16]. Taken together, these constraints reinforce the view that Vesta underwent rapid core formation and magma ocean crystallization very early in Solar System history, within just a few million years of CAI formation.

Conclusion: Our VMO crystallization model suggests that the core of Vesta formed at ~1 Myr after CAI formation, and that the subsequent crystallization of the magma ocean was completed within ~1 Myr. These estimates are consistent with previous studies and support the idea that the presence of short-lived ²⁶Al was the primary heat source driving early differentiation. Our model estimated the formation depths of the source materials of HED meteorites from the Nd isotopic distributions estimated by this model. In reality, however, HED meteorites were generated through later processes such as partial melting and impact excavation. Thus, the observed Nd isotopic signatures in HEDs represent a combination of primary mantle stratification and subsequent geological modification. Looking ahead, it will be necessary to incorporate the effects of partial melting and impact processes into the model, so that not only Nd isotopic systematics but also petrological and geochemical features of HED meteorites can be consistently explained. This will allow for a more comprehensive understanding of Vesta's evolutionary history. This model provides new constraints on Vesta's evolutionary timescale and internal structure, and further integration with other isotope systems will help refine the mechanisms of its accretion and differentiation. Nonetheless, the available Nd isotope data for HED meteorites remain limited, and additional high-precision measurements will be essential to fully test and refine these conclusions.

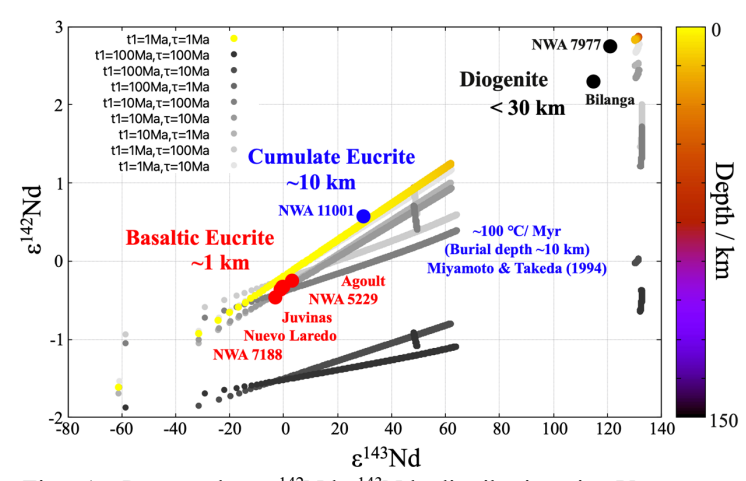


Fig. 1. Present-day ε^{142} Nd- ε^{143} Nd distribution in Vesta, as estimated from VMO crystallization model, compared with HED meteorite [12,13]. τ : timescale of VMO crystallization, t_1 : core formation timing.

Table 1. Assumed constituent minerals of Vesta.

Depth from surface	Constituent minerals				
0-15 km	Clino-Pyroxene 60 %, Plagioclase 40 %				
$15\text{-}60~\mathrm{km}$	Olivine 10 %, Ortho-Pyroxene 90 %				
60-150 km	Olivine 90 %, Ortho-Pyroxene 10 %				

Table 2. Used value in this calculation [8-12].

Variable	Value	Variable	Value
$\lambda_{142 ext{Nd}}$	$0 \ { m year}^{-1}$	$(^{142}{ m Nd}/^{144}{ m Nd})_{ m SSI}$	1.141539
$\lambda_{143 ext{Nd}}$	$0 \ { m year}^{-1}$	$(^{143}{ m Nd}/^{144}{ m Nd})_{ m SSI}$	0.506674
$\lambda_{146\mathrm{Sm}}$	$6.73e-9 \ { m year}^{-1}$	$(^{146}{ m Sm}/^{144}{ m Sm})_{ m SSI}$	0.008
$\lambda_{147\mathrm{Sm}}$	$6.54e-12 \text{ year}^{-1}$	$(^{147}\mathrm{Sm}/^{144}\mathrm{Nd})_{\mathrm{Present}}$	0.196
$^{144}\mathrm{Nd}/\mathrm{Nd}$	0.2383	$(^{142} \text{Nd}/^{144} \text{Nd})_{\text{std}}$	1.141840
$^{144}\mathrm{Sm/Sm}$	0.0307	$(^{143}{ m Nd}/^{144}{ m Nd})_{ m CHUR}$	0.512638

SSI = Solar System initial isotopic ratio. CHUR = Chondritic Uniform Reservoir.

References: [1] Greenwood R. C. et al. (2014) *EPSL*, 390, 165–174. [2] Warren, P.H. (1997) *Meteorit. Planet. Sci.*, 32, 945–963. [3] Debaille V. M. et al. (2007) *Nature*, 450, 525–528. [4] Yamazaki S. and Mikouchi T. (2025) 87th *MetSoc*, #5188. [5] Kleine T. et al., (2004) *GCA*, 68, 2935-2946. [6] Schiller M. et al., (2011) *The Astrophys. Jour. Lett.*, 740, L22. [7] Miyamoto M. and Takeda H. (1994) *Meteoritics*, 29, 505. [8] Jacobsen S. B. and Wasserburg G. J. (1980) *EPSL*, 50, 139-156. [9] Marks N. C. et al. (2014) *EPSL*, 405, 15-24. [10] Rosman K. J. R. and Taylor P. D. P. (1998) *Pure Appl. Chem.*, 70, 217-235. [11] Amelin Y. M. and Rotenberg E. (2004) *EPSL*, 223, 267-282. [12] Jacobsen S. B. and Wasserburg G. J. (1980) *EPSL*, 50, 139-155. [13] Kagami S. et al. (2016) 47th *LPSC*, #2235. [14] https://ir.lib.uwo.ca/etd/6594/?utm_source=ir.lib.uwo.ca% 2Fetd%2F6594&utm_medium=PDF&_campaign=PDFCoverPages. [15] Yamazaki S. and Mikouchi T. (2025) 56th *LPSC*, #1892. [16] Takeda H. (1997) *MAPS*, 32, 841-853.

The "hot shock" hypothesis for the formation of quenched angrites: Evidence from olivine xenocrysts in NWA 13363

Hideyuki Hayashi¹, Rikuto Honda² and Takashi Mikouchi³
¹Department of Science, National Museum of Nature and Science
²Department of Earth and Planetary Science, University of Tokyo
³University Museum, University of Tokyo

Introduction:

Angrites are one of the oldest diffenentiated meteorites, derived from the crust of protoplanet in the early solar system. Angrites show two distinct textures: quenched or slowly-cooled. Among them, quenched angrites have older crystallization ages of ~ 4564 Ma (e.g., Amelin, 2008). Thus, quenched angrites preserve the earliest processes of protoplanetary crustal formation.

The formation process of quenched angrites remains poorly understood. Their rapid cooling rates suggest that they were quenched near the surface of the parent body (Mikouchi *et al.*, 2001), but the specific geological processes remain unclear. There are two theories regarding the formation process of angrite melt: the impact melting model (e.g., Jambon *et al.*, 2008) and the partial melting model (e.g., Keil, 2012).

Quenched angrites typically contain olivine xenocrysts that are Mg-rich and chemically homogeneous within individual grains, but heterogeneous between grains. Moreover, both deformed and undeformed xenocrysts coexist in a single sample, as reported for Asuka-881371, Asuka 12209, D'Orbigny, and Northwest Africa (NWA) 12320 (e.g., Mikouchi, 1996). The oxygen isotopic compositions of olivine xenocrysts are within the angrite fractionation line (AFL) (Hayashi *et al.*, 2020a; Rider-Stokes *et al.*, 2023), suggesting that they crystallized within the angrite parent body (APB).

In this study, we focus on olivine xenocrysts in quenched angrite NWA 13363, based on petrological and mineralogical observations, and propose a new "hot shock" hypothesis for the formation of quenched angrites.

Sample and analytical methods:

We conducted mineralogical investigations of NWA 13363. NWA 13363 was found in Algeria in 2020 with the total mass of 54 g. Thin sections of NWA 13363 were examined using an optical microscope. Textural observations and chemical compositional analyses were conducted with an electron probe microanalyzer (JEOL JXA-8200 at the National Institute of Polar Research and JEOL JXA-8230 at the National Museum of Nature and Science). Phase identification of minerals was performed using a microscopic Raman spectrometer (Photon Design) at the National Museum of Nature and Science.

Results:

The matrix of NWA 13363 mainly consists of olivine, anorthite, and clinopyroxene, and exhibits an ophitic texture. Olivine phenocrysts, typically $\sim 200~\mu m$ in size, display rounded shapes and compositions ranging from Fo₆₇Fa₃₂La₁ \sim Fo₀Fa₈₂La₁₈ \sim Fo₅Fa₅₇La₃₈. On the other hand, six olivine xenocrysts were found in the thin sections. Four large grains are $\sim mm$ in size, and one large xenocryst exhibits a mosaic texture (Fig. 1). Chemical compositions of large olivine xenocrysts are Fo₈₃, Fo₈₄, Fo₈₄ and Fo₈₈Fa₁₂La₀ \sim Fo₇₅Fa₂₂La₃ (mosaic olivine). The rest of olivine xenocrysts are recognized as cores within the olivine phenocrysts (Fo₈₁, Fo₈₅).

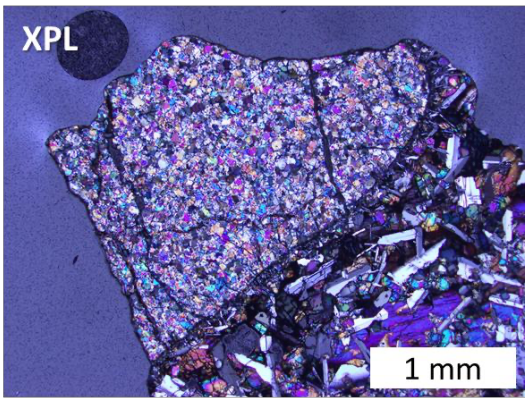


Fig. 1. Photomicrograph (xpl) of mosaic olivine.

The mosaic olivine shows a recrystallized texture, consisting of fine-grained recrystallized olivine (20–100 μ m) with random orientations. The compositions of recrystallized olivines vary from Fo₈₈ at the core to Fo₇₅ at the rim. Grain boundaries of recrystallized olivines are filled with diopside (Mg# = 82), irregular vesicles up to ~30 μ m, and minor chromite and Ni-bearing troilite. Phenocrysts in the matrix crystallize outward from the xenocryst surface with mosaic olivine xenocrysts as crystallization seeds.

Cooling rates recorded in two homogeneous Fo₈₄ xenocrysts were estimated from the Fe-Mg diffusion profiles

(Miyamoto *et al.*, 2002), assuming linear cooling from 1400 °C to 900 °C. The results yielded $60 \sim 210$ °C/hr. Although precise cooling rates could not be determined for the mosaic xenocryst, the Fe-Mg diffusion between recrystallized olivines suggests similar rates to those of the homogeneous xenocrysts. We made a simple estimate using a software called DIPRA (Girona and Costa, 2013). By linking the initial Fo# with the profile of CaO wt%, and assuming the temperature at which diffusion occurred to be 1200 °C, we can estimate that the diffusion occurred about 20 minutes.

Discussion and Conclusion:

Oxygen isotope compositions of olivine xenocrysts plot within the AFL indicating crystallization within the angrite parent body (Hayashi *et al.*, 2020a; Rider-Stokes *et al.*, 2023). Although Mg-rich compositions resemble mantle-derived olivine (Jambon *et al.*, 2008), xenocrysts in quenched angrites do not occur as xenoliths but exclusively as rounded single crystals. This texture suggests that they were equilibrated as individual crystals suspended in melt in the APB.

However, some xenocrysts record compositional modification at only around rim. This indicates that they were incorporated into the melt and quenched before achieving equilibrium.

Traditional models for formation process of angrite melt (the impact melting model and the partial melting model) face difficulties. The partial melting model can explain deformed grains under high P–T conditions (e.g., Trepmann *et al.*, 2013), but cannot account for completely recrystallized mosaic olivine, absence of dunite xenoliths, or observed oxygen isotope heterogeneity of the groundmass (Rider-Stokes *et al.*, 2023). The impact melting model faces the problem that impact breccias are rare among quenched angrites (only NWA 15861; Irving *et al.*, 2023). Furthermore, attributing mosaic and deformed olivine to impact residues fails to explain the coexistence of undeformed Mg-rich olivine in the same samples.

To resolve these issues, we propose the "hot shock" hypothesis (Fig. 2). This model, previously hinted by noble gas analyses of NWA 7203 quenched angrites (Takenouchi *et al.*, in review), lacked petrographic evidence. We suggest that the APB was largely molten, with only a thin crust. Olivine, in equilibrium with melt, was suspended in the magma ocean. Under the influence of a metallic core, such olivine could be Mg-rich and rounded single crystal such as pallasites. Thus, Mg-rich olivine of varying compositions could coexist depending on depth or melt composition.

If a positive $\Delta^{17}O$ (= $\delta^{17}O$ - 0.52 $\delta^{18}O$) impactor (Rider-Stokes *et al.*, 2023) struck this partially molten parent body, olivine xenocrysts would have experienced variable shock metamorphism depending on distance from the impact site. These xenocrysts were subsequently incorporated into angritic melts, some of which erupted near the surface, cooled rapidly, and crystallized with varial cooling rates depending on burial depth, producing the observed textural variations (Hayashi *et al.*, 2020b).

Future work will involve shock deformation experiments on olivine in melt to test whether shock textures in quenched angrites can be reproduced, as well as crystallization experiments of Mg-rich olivine with angritic melts under coexistence of Fe metal melt. Comparisons with olivine in pallasite will further constrain the "hot shock" hypothesis for the formation of quenched angrites.

silicate melt metal melt

Fig. 2. The schematic illustration of "hot shock".

References

Amelin Y, Geochimica et Cosmochimica Acta 72, 221-32, 2008. Girona T, Costa F, Geochemistry, Geophysics, Geosystems, 14, 422-431, 2013. Hayashi H, Kim NK, Kim H et al., Goldschmidt Conference, 2020a. Hayashi H, Mikouchi T, Yamaguchi A, The 11th Symposium on Polar Science, 2020b. Irving AJ, Carpenter PK, Bekaert D et al., 86th Annual Meeting of the Meteoritical Society, 6121, 2023. Jambon A, Omar B, Michel F et al., Meteoritics and Planetary Science, 43, 1783-1795, 2008. Keil K, Chemie der Erde-Geochemistry 72, 191-218, 2012. Mikouchi T, Miyamoto M, McKay G, Proceedings of NIPR Symposium on Antarctic Meteorites, 9, 174-188, 1996. Mikochi T, Miyamoto M, McKay G, Le L, Meteoritics and Planetary Science, 36, A131-135, 2001. Miyamoto M, Mikouchi T, Arai T, Antarctic Meteorite Research, 15, 143-151, 2002. Trepmann CA, Renner J, Druiventak A, Solid Earth Discuss, 5, 463–524, 2013. Rider-Stokes BG, Greenwood RC, Anand M et al., Nature astronomy, 7, 836-842, 2023.

Mineralogical characteristics of the plagioclase xenocryst in a quenched angrite: Link between quenched and slowly-cooled angrites?

<u>Rikuto Honda</u>¹, Hideyuki Hayashi², Sojiro Yamazaki¹, Ben G. Rider-Stokes³, Akira Yamaguchi⁴ and Takashi Mikouchi⁵

¹Dept. Earth and Planet. Sci., University of Tokyo, Tokyo 113-0033, Japan (honda-rikuto@g.ecc.u-tokyo.ac.jp)

²Dept. of Science, National Museum of Nature and Science (NMNS), Tsukuba, Ibaraki 305-0005, Japan

³School of Phys. Sci., The Open University, Milton Keynes, UK

⁴National Institute of Polar Research (NIPR), Tachikawa, Tokyo 190-0014, Japan

⁵University Museum, University of Tokyo, Hongo, Tokyo 113-0033, Japan

Introduction: Angrites are some of the most ancient achondrite meteorites [e.g., 1] and are divided into two major sub-groups based on their petrographic textures: the quenched and slowly-cooled angrites[2]. Quenched angrites show rapidly crystallized textures and older crystallization ages in contrast to the slowly-cooled angrites. In addition, they are known for often having millimeter-sized olivine and/or spinel xenocrysts [e.g., 3]. On the other hand, slowly-cooled angrites exhibit granular and/or cummulate textures, and the constituent minerals have relatively homogenous compositions. So far, the petrogenetic relationship between these two groups has never been established because their petrographic characteristics and crystallization ages differ distinctly from each other.

In this situation, we pay attention to Northwest Africa (NWA) 12879, which is classified as a quenched angrite based on its petrographic texture [4], as we found that it contains a plagioclase megacryst. In this abstract, we report on the petrology, mineralogy, and oxygen isotopic composition of NWA 12879 and question whether the plagioclase megacryst is a xenocrystic in nature or not. Based on the results, we discuss the origin and mineralogical characteristics of the plagioclase megacryst and discuss the relationship with slowly-cooled angrites.

Sample and Methods: We prepared polished thin sections of NWA 12879 (~1 x 1 cm), 7 quenched and 5 slowly-cooled angrites, and observed the samples by an optical microscope and FE-SEM (JSM-7000F at Univ. of Tokyo; JSM-7100F at NIPR). Mineral compositions were acquired using EPMA (JEOL JXA-8200 at NIPR: JEOL JXA-8230 at NMNS) and FE-EPMA (JEOL JXA-8530F at Univ. of Tokyo). Oxygen isotopic composition of NWA 12879 was measured by laser-assisted fluorination at the Open Univ., following established procedures in [e.g., 5].

Results: NWA 12879 demonstrates a highly fine-grained ophitic texture (Fig. 1a), and its constituent minerals are mostly pure anorthite (An_{98.7-100}), Al-Ti-Cpx (Fs_{18.8-47.1}Wo_{49-54.5}, Al₂O₃ 3.4-8.5 wt.%, TiO₂ 0.7-5.1 wt.%, Fe/Mn=59-199), Ca-bearing olivine (with kirschstainite: Fo_{0.4-69.3}Ln_{1.1-34}, Fe/Mn=53-106), together with accessory troilite, spinel, silico-apatite, Al-Ti-free Cpx, relatively Na-rich plagioclase (up to An_{89.9}Ab_{9.5}), rare Fe-oxide, and celsian. Anorthite and Al-Ti-Cpx show undulatory extinction under optical microscopy observations. Al-Ti-Cpx and olivine exhibit extensive chemical zoning. Additionally, olivine often shows intergrowth with kirschstainite. As possible xenocrysts, there are many small grains of olivine (up to ~300 μm) with Mg-rich cores (Fo₇₉₋₈₈) compared with the phenocrysts, similar to other quenched angrites [e.g., 3]. In addition, NWA 12879 contains a plagioclase megacryst (Fig. 1b: ~1.8 mm). Its size is distinctly larger than that of the phenocrysts (up to ~200 μm), and it is rounded in shape and has a sharp boundary with the matrix. However, it has a pure anorthite composition ($An_{99,1-100}$), which is the same as the phenocrystic anorthite. Additionally, the plagioclase megacryst has a vein-like texture with olivine and Al-Ti-Cpx, which have continuous compositions with the groundmass phases (Olivine: Fo_{0.4-35}Ln_{4.8-37.4}, Fe/Mn=62-91; Al-Ti-Cpx: Fs_{20,2-47.0}Wo_{51,6-54.1}, Al₂O₃ 5.2-7.7 wt.%, TiO₂ 1.3-4.5 wt.%, Fe/Mn=58-162), and there are many small and rounded anorthite grains in this texture. On the other hand, the Fe-Mg compositional trend of the plagioclase megacryst differs from the anorthite phenocrysts (Fig. 2). Also, the Fe content is richer at the rim than at the core. The oxygen isotopic composition of NWA 12879 is still in progress, and so the data will be presented at the symposium.

Discussion and Conclusion: From our analysis of the petrography and constituent mineral composition of NWA 12879, we consider it to be a queched angrite as initially characterized [4]. However, the plagioclase megacryst contained has never been reported from other quenched angrites. The major elemental compositions of the plagioclase megacryst are identical to phenocrystic anorthite. On the other hand, the Fe and Mg compositional trend

and petrographic texture distinctly differ from the phenocrystic anorthite. Therefore, we consider the plagioclase megacryst to be a xenocryst, similar to olivine and spinel xenocrysts, which are observed in other quenched angrites [e.g., 3]. We believe that it is from the angrite parent body (APB) because pure anorthites (An₁₀₀) are hardly recognized in other achondrites [e.g., 6]. In fact, large and rounded anorthites are common in slowly-cooled angrites, such as BiZ 011 and NWA 16129 [4, 7]. Especially, the large anorthite grains in BiZ 011 often contain vein-like olivine and Cpx associated with small and rounded grains of anorthite [7], which is the same as the plagioclase xenocryst. However, olivine in the plagioclase xenocryst exhibits intergrowth with kirschstainite, whereas in BiZ 011, it displays an exsolution texture with kirschstainite [7]. We consider it is due to the difference of their cooling rates, as the cooling rate of quenched angrites is > 3 °C/h [8], while that of slow-cooled angrites is $\sim 0.01-0.25$ °C/yr As seen in Fig. 2, the Fe and Mg compositional trend of the plagioclase xenocryst differs from those of quenched and slowly-cooled angrites. However, its Fe content matches that of slowly-cooled samples except for its rim composition, and its Mg composition is close to the phenocrystic anorthite of NWA 12879 and other quenched angrites. Assuming the original composition was similar to that of slowly-cooled angrites, and it was changed due to atomic diffusion, we can roughly estimate the duration in which the plagioclase xenocryst was incorporated in the parent melt of NWA 12879 using the Mg diffusion coefficient of plagioclase and the diffusion formula: $L^2=2Dt$. Where L is a distance, and t is a time. Assuming the diffusion distance is 0.9 mm, the initial temperature is 1550 $^{\circ}$ C [10], and the Mg diffusion coefficient is 10^{-14} [11], the minimum duration is ~1.3 days. It does not contradict the considered duration deduced from olivine xenocryst [e.g., 8]. So far, however, we do not know if the original composition of plagioclase xenocryst was similar to anorthite in slowly-cooled angrites.

This is the first report of a plagioclase xenocryst in a quenched angrite. We consider that it may be a link between quenched and slowly-cooled angrites because it has some mineralogical similarities to the anorthite in some slowly-cooled angrites. It suggests the possibility that minerals like those contained in slowly-cooled angrites were already present when quenched angrites formed, and/or quenched angrites still crystallized when slowly-cooled angrites formed. However, to confirm and develop this idea, we need to analyze anorthite in angrites in more detail, for example, crystallization ages and trace element abundance of NWA 12879 and BiZ 011.

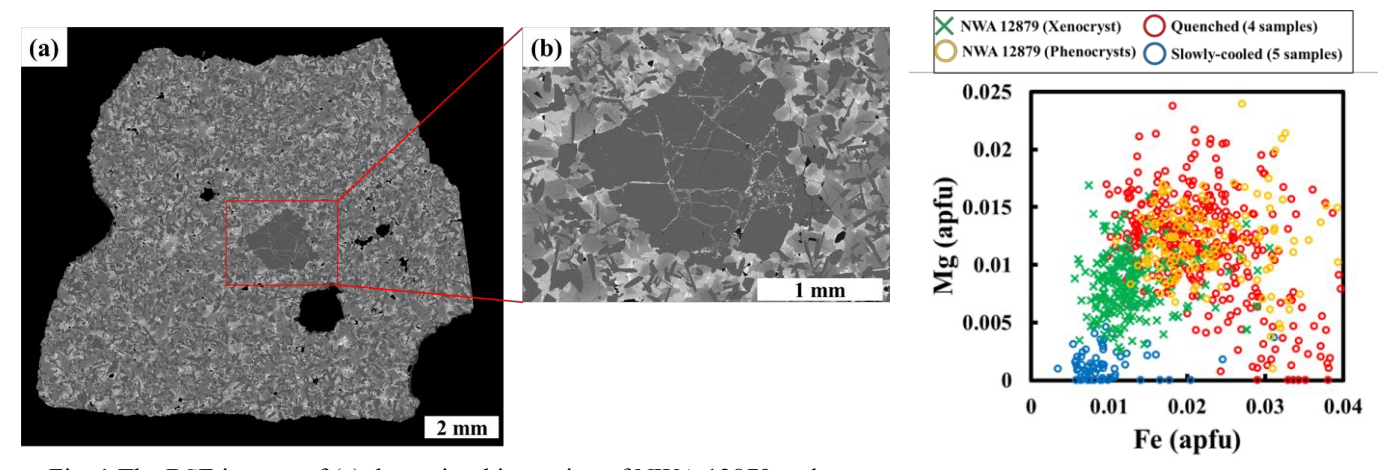


Fig. 1 The BSE images of (a) the entire thin section of NWA 12879 and (b) plagioclase megacryst.

Fig. 2 Fe vs. Mg content of anorthite in angrites.

References

[1] Kleine T. et al. (2012) Geochim. Cosmochim. Acta, 84, 186–203. [2] Keil K. (2012) Chemie der Erde, Geochem., 72, 191-218. [3] Mittlefehldtl D. W. et al. (2002) Meteorit. & Planet. Science, 37, 345-369. [4] Meteoritical Bulletin Database (https://www.lpi.usra.edu/meteor/metbull.cfm) [5] Rider-Stokes B. G. et al. (2023) Nature Astron., 7, 836-842. [6] Krot G. et al. (2014) Reference Module in Earth Systems and Environ. Sciences, 1, 1-63. [7] Honda R. and Mikouchi T. (2025) Lunar Planet. Sci. LVI, Abstract # 2164. [8] Hayashi H. (2021) Doctoral Dissertation. [9] Honda R. et al. (2025) 87th Annual Meeting of Meteorit. Soc., id.5222. [10] Goldsmith J. R. (1980) American Mineral., 65, 272-284. [11] Cherniak D. J. (2010) Rev. in Mineralogy & Geochem., 72, 691-733.

The chemical compositions of Asuka and Yamato iron meteorites, and their classification

Naoki Shirai¹, Akira Yamaguchi² and Mitsuru Ebihara²

¹Kanagawa University, ²National Institute of Polar Research, ³Tokyo Metropolitan University

Introduction

Iron meteorites provided essential information on the differentiation and crystallization processes of their parent bodies. The classification of iron meteorites is based on trace element abundances and structures. More than 1400 iron meteorites have been recovered to date, of which about 60% belong to IAB and IIIAB irons, followed by over 10% in IIAB irons. In addition, more than 10% of iron meteorites are classified as ungrouped, whose chemical compositions differ from those of the thirteen established chemical groups. Among the iron meteorites recovered from Antarctica, IAB and IIIAB are also the most abundant groups. However, unlike non-Antarctic iron meteorites, 39% of the Antarctic iron meteorites were reported to be ungrouped [1]. Since then, the number of Antarctic iron meteorites has increased to more than 200, with over half of them recovered after 1990. A similar trend is observed for the meteorites recovered near the Yamato Mountains, where 23 of the 37 Yamato iron meteorites have been discovered since 1998.

The objective of this work is to determine the chemical compositions of 12 Asuka iron meteorites and 28 Yamato iron meteorites for their classification. We also aim to examine the origin of the ungrouped Yamato iron meteorites and compare the group distribution of iron meteorites recovered from the Balchen, Nansen ice fields and Yamato Mountains with that of non-Antarctic iron meteorites.

Experiments

12 Asuka and 28 Yamato iron meteorites were investigated in this study. Some of the iron meteorites were analyzed by using both LA-ICPMS and INAA to confirm whether our LA-ICP-MS data represent the representative chemical compositions. INAA was performed at Institute for Integrated Radiation and Nuclear Science, Kyoto University. LA-ICPMS analysis was carried out using a Thermo ElementXR coupled to CETAC LSX-213 at NIPR. Iron meteorites were ablated on line mode with spot size of 100 μm at a scan speed rate of 25-50 μm/s. All analyses were performed with 20Hz repetition rate and 100% power output. Under these conditions, ³¹P, ⁵³Cr, ⁵⁷Fe, ⁵⁹Co, ^{60, 61, 62}Ni, ^{63, 65}Cu, ^{69, 71}Ga, ^{73, 74}Ge, ⁷⁵As, ⁹⁵Mo, ^{101, 102}Ru, ¹⁰³Rh, ^{105, 106}Pd, ^{182, 183, 184}W, ^{185, 187}Re, ^{189, 190}Os, ^{191, 193}Ir, ^{194, 195}Pt and ¹⁹⁷Au were monitored in low resolution (R = ~300). Three to five separates lines were selected by avoiding inclusions of troilite and schreibersite and analyzed. For quantification, North Chile (IIAB), Hoba (IVB), NIST SRM 663 are used as reference samples. Elemental abundances were determined from more than two isotopes for some elements, average values are calculated.

Results and Discussion

For classification, plots of Co, Ni, Cu, Ga, Ge, As, W, Re, Ir, and Pt vs. Au were used along with the structures. *Asuka Iron meteorites:* Among the twelve Asuka iron meteorites analyzed, three were classified as IIIAB, one as IID, one as IVA, one as IIE, two as IIIE, and three as IAB. According to the classification scheme of Wasson [2], IIR irons can be subdivided into Main IIE and Cu-(or FeS) rich IIE. A-881818 was assigned to the Cu-(or FeS) rich IIE subgroup. Three meteorites, A-87263, A-881111, and A-882112, were classified as IAB. Based on the Ni vs. Au plot, IAB irons are subdivided into the main group and five subgroups [3]. A-87263 falls into IAB-sLH, A-88111 into IAB-sLL. A-882112 plots within the IAB-sLL iron field in the Ni vs. Au diagram. However, this meteorite falls between IAB-sLL and IAB-sLM in the W vs. Au and Ir vs. Au plots. Therefore, A-882112 was assigned to be IAB-sLL-an.

Yamato Iron meteorites: Among the 28 Yamato iron meteorites analyzed in this study, 14 were classified as IAB, one as IIAB, four as IIIAB, one as IVA, and the remaining eight as ungrouped. Y 000703, assigned to IIIAB, shows chemical compositions and structure identical to those of Y 000311, indicating that Y 000703 is a pair of Y 000311. Among the 14 meteorites classified as IAB, Y 980517 was assigned to IAB-sLH, while Y 003569 and Y-794206 plot within the fields of IAB-sLH and IAB-sHL irons, respectively, in the Ni vs. Au diagram. However, Y 003569 shows lower concentrations of As, Ge, and Ir compared with IAB-sLH, and is therefore classified as IAB-

sLH-an. Y-794206 shows higher Co and Cu and lower Ga compared with IAB-sHL, and is thus classified as AIB-sHL-an. The remaining 11 meteorites were classified as IAB-ungrouped.

Among the ungrouped irons, Y 983934, Y 000088, and Y 000090 are characterized by low Co and high Si contents, resembling metal fractions of enstatite chondrites and achondrites. Y 983934 shows flat CI-normalized siderophile and chalcophile elements abundances, consistent with the metal fraction of enstatite chondrite. In contrast, Y 000088 and Y 000090 are depleted in refractory siderophile elements but not in moderately or volatile siderophile elements, indicating that they represent metal fractions of enstatite achondrites formed by partial melting. Y-792345, Y-82003, and Y-86267 have low P abundances, comparable to metal fractions of ordinary chondrites. Their CI-normalized moderately and volatile siderophile elements are similar to those of bulk H chondrite metal, but highly siderophile elements are strongly depleted. These characteristics, also seen in large metal nodules of ordinary chondrites and some iron meteorites (e.g., ALH 84233, LEW 88023), indicate that Y-792345, Y-82003, and Y-86267 represent a metal fraction of H ordinary chondrite. Y-791836 is distinguished by extremely low Ga and Ge abundances and relatively high P and Cr. Its CI-normalized siderophile elements show chondritic pattern for refractory elements, but strong depletion in Cu, Ga and Ge. These chemical characteristics can be seen in other ungrouped iron meteorites, however, these ungrouped iron meteorites are depleted in As and Au relative to Y-791836. The chemical composition of Y 983805 does not match those of any ungrouped iron meteorites.

Group distribution of Asuka and Yamato iron meteorites: In the Balchen and Nansen ice fields, and Yamato Mountains, where Asuka and Yamato iron meteorites were recovered, IAB and IIIAB account for 50 to 60%, consistent with the proportions observed in non-Antarctic iron meteorites. No ungrouped irons have been identified in Asuka iron meteorites, whereas about 30% of Yamato iron meteorites are classified as ungrouped. Six Yamato iron meteorites analyzed in this study are considered to be metal fractions of enstatite chondrites and achondrites, as well as metal fractions of ordinary chondrites. When these six Yamato iron meteorites are excluded, the proportion of ungrouped iron meteorites from Yamato Mountains decreases to 16%, which is comparable to that of non-Antarctic iron meteorites.

References

[1] Wasson J.T. (1990) Science 249: 900-902. [2] Wasson J.T. (2017) GCA 197: 396-416. [3] Wasson J.T. and Kallemeyn G.W. (2002) GCA 66:2445-2473.

Contrasting Roles of Water During Late- and Post-Igneous Crystallization of Lunar vs. Terrestrial Gabbros: NWA 773 Clan of Lunar Meteorites vs. Murotomisaki Gabbroic Sill, Japan

<u>Timothy J. Fagan¹*</u> and Fugo Hattori¹

Dept. Earth Sciences, Waseda University, Tokyo, Japan (*fagan@waseda.jp)

Based on Apollo era work and for several years following, rocks from the Moon were considered anhydrous, and the role of water during formation and geological evolution of the Moon was considered minimal. A dramatic shift in perspective allowing a more active role of H₂O in the origin of lunar rocks stemmed from the discovery of hydrogen in lunar glasses and melt inclusions in olivine by Saal, Hauri and co-workers [1,2]. Subsequent analyses of lunar samples have shown that water, in some form, was probably an active geochemical agent during formation of some lunar rocks (see reviews of [3,4]).

In this study, we compare the roles of water in late-stage igneous rocks from: (1) the Northwest Africa 773 (NWA 773) clan of lunar mafic meteorites [5,6] with (2) the Murotomisaki gabbroic sill (MGS) from Shikoku Island, Japan [7,8]. Because H₂O is incompatible in mafic silicate igeous systems, if H₂O is initially present, it is likely to be concentrated in late-stage rocks that are enriched in incompatible elements. Thus by focusing on late-stage rocks, we enhance our chances of finding rocks that were affected by a hydrous species during igneous crystallization. We find that though some water was likely present during crystallization of NWA 773, the effects of water are much more dramatic in the MGS, indicating higher pressures of H₂O during and following igneous crystallization.

Samples and Methods: Textures and compositions of minerals and glass were determined from polished thin sections (pts) from the NWA 773 clan and the MGS. Analyses are from two pts of NWA 773, two pts of NWA 2977, and one pts from the MGS. The MGS sample, labelled Muro-14, is a very coarse pyroxene-plagioclase gabbro collected from the Middle Zone of the MGS, which is the last major unit of the MGS to form during igneous crystallization based on field and petrologic studies [7,8]. An olivine cumulate gabbro (OCG) is typical of the NWA 773 clan [5,6]; NWA 2977 is an unbrecciated sample consisting entirely of OCG, whereas NWA 773 is a breccia with a variety of clasts, including OCG.

Textures of the samples were described based on imaging from petrographic microscopes, and elemental and back-scattered electron (BSE) maps. Elemental and BSE maps were collected using a JEOL JXA-8900 electron probe micro-analyzer (EPMA) at the Waseda University Department of Earth Sciences (WU). Quantitative elemental compositions of minerals and glass were analyzed by wavelength dispersive spectroscopy using the WU EPMA. Well-characterized silicates, oxides and phosphates were used as standards. Typical analyses were collected using a 15 kV, 20 nA electron beam, counting for 10 s on peaks and 5 s on two backgrounds

To evaluate potential losses of Na during EPMA of feldspar, we conducted replicate analyses of test feldspars with beam rastering at $100,000 \mathrm{X}$ ($\sim 1~\mu \mathrm{m}$ diameter spot) and $20,000 \mathrm{X}$ ($6x8~\mu \mathrm{m}$ spot). Ab-rich feldspar ($Ab_{90}An_{10}$) is more susceptible to Na-loss during EPMA than An-rich feldspar ($Ab_{45}An_{54}$); however, use of the $6x8~\mu \mathrm{m}$ spot minimizes Na-loss during the first two replicate analyses of even Ab-rich feldspar (Fig. 1). The $6x8~\mu \mathrm{m}$ spot was used for feldspar analyses in this study.

Results and Discussion: Relatively fine-grained, incompatible element-rich pockets were found trapped between cumulus minerals in both the MGS (Fig. 2) and NWA 773 OCG. An additional late-stage lithology in the OCG occurs as alkali-rich phase ferroan clasts [5]. Plagioclase feldspar crystals in both the MGS and OCG exhibit discontinuous zoning. Feldspar adjacent to pockets in the MGS has been albitized as a result of post-igneous coupled dissolution-precipitation reactions with hydrous fluid [9]. Further evidence of post-igneous crystallization with aqueous fluid is provided by H₂O-bearing minerals such as prehnite, biotite and chlorite in MGS pockets (Fig. 2). Some feldspar crystals adjacent to pockets in the NWA 773 OCG also exhibit a discontinuous drop in Ancontent with proximity to the pockets, but at higher An-contents (An₋₉₀ to An₋₈₀). We suggest that the drop in Ancontent of plagioclase in the OCG is due to precipitation of Ca-phosphates in the pockets and consequent lowering of Ca concentration in co-existing igneous liquid. Preliminary analyses suggest that all apatite in Muro-14 and some apatite in OCG have some OH., suggesting that H₂O was present in some form when the OCG pockets

crystallized. Nonetheless, water pressures were much higher during and after igneous crystallization of Muro-14. Textural replacement of biotite by chlorite indicate that K was lost from the MGS pockets during post-igneous crystallization. Thus, the NWA 773 OCG pockets are more likely to preserve the true K-rich compositions of late-stage igneous origin.

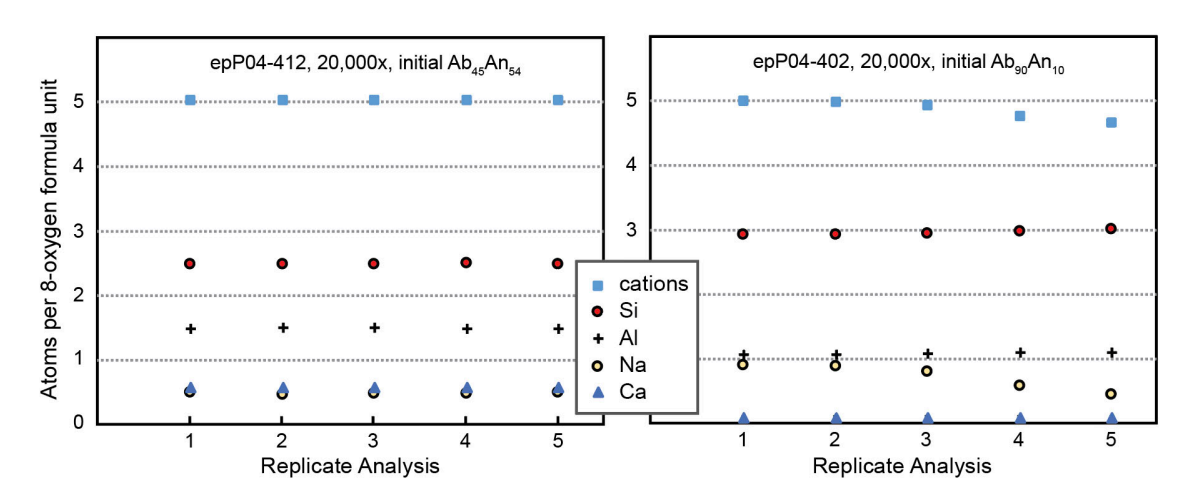


Figure 1. Replicate analyses to test for Na-loss during EPMA of $Ab_{45}An_{54}$ and $Ab_{90}An_{10}$ feldspars. The electron beam was exposed to the sample for 180 s during each replicate; the Faraday cup was closed for 10 s between replicates. With the beam rastering at 20,000x, the spot size is approximately $6x8 \mu m$.

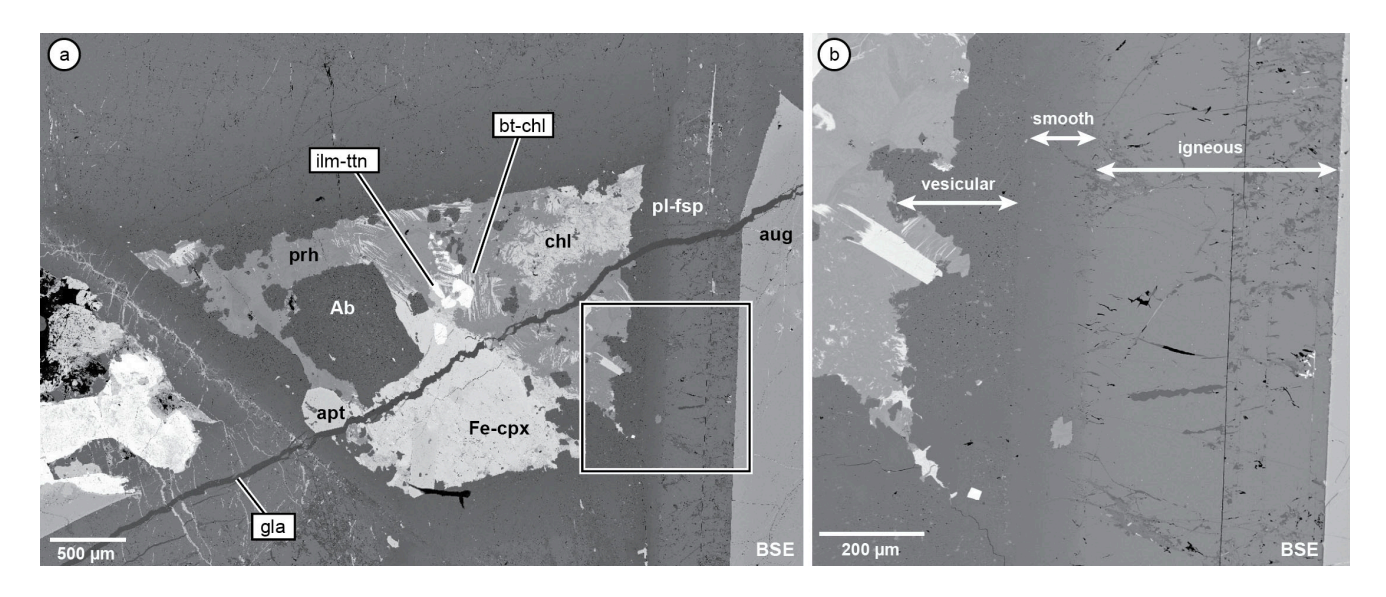


Figure 2. BSE images of an incompatible element-rich pocket in MGS sample Muro-14. Box in (a) is shown in detail in (b). Plagioclase crystals adjacent to pocket have vesicular $(Ab_{>90})$ and smooth $(Ab_{>85})$ textural varieties of albitized feldspar (b). "Igneous" feldspar exhibits minor zoning from core $(An_{59}Ab_{40})$ to rim $(An_{54}Ab_{46})$ and is albitized along BSE-dark fractures. Abbreviations: Ab = albite; apt = apatite; aug = augite; bt = biotite; chl = chlorite; Fe-cpx = ferroan high-Ca pyroxene; gla = alkali-rich glass vein; ilm-ttn = ilmenite with titanite; pl-fsp = plagioclase feldspar; prh = prehnite.

References: [1] Saal A.E. et al. (2008) Nature 454: 192-195. [2] Hauri E.H. et al. (2011) Science 333: 213-215. [3] Robinson K.L. and Taylor G.J. (2014) Nature Geoscience 7: 401-408. [4] McCubbin F.M. et al. (2023) Reviews in Mineralogy & Geochemistry* 89: 729-786, *New Views of the Moon 2, edited by Neal C.R. et al. [5] Fagan T.J. et al. (2014) Geochimica et Cosmochimica Acta 133: 97-127. [6] Valencia S.N. et al. (2019) Meteoritics and Planetary Science 54: 2083-2115. [7] Hoshide T. et al. (2006) Journal of Mineralogical and Petrological Sciences 101: 223-239. [8] Hoshide T. and Obata M. (2012) Journal of Petrology 53: 419-449. [9] Engvik A.K. et al. (2008) Canadian Mineralogist 46: 1401-1415.

A potential two-billion-year-old KREEP-rich lunar meteorite, Northwest Africa 16895.

Mizuho Koike¹, Ryosuke Sakai¹, Ryoichi Nakada², Ben G. Rider-Stokes³, Kohei Sasaki⁴, and Naoto Takahata⁴

¹Earth and Planetary Systems Science Program, Hiroshima University.

²Kochi Institute for Core Sample Research, Japan Agency for Marine-Earth Science and Technology.

³School of Physical Sciences, The Open University.

⁴Atmosphere and Ocean Research Institute, The University of Tokyo.

Introduction: Northwest Africa (NWA) 16895 was found in Algeria in 2023 and was initially categorized as a martian augite basalt based on its petrology [1]. However, our mineralogical and geochemical analyses of this meteorite as well as U–Pb chronological data [2] pose a question about its origin. At this moment, we speculate that NWA 16895 may be one of the youngest KREEP-rich lunar basalts. The latest understanding of this meteorite and its potential implication will be presented at the symposium.

Sample & Methods: A small slice of NWA 16895 was cut and embedded in epoxy resin to make a polished section. The sample was briefly observed under an optical microscope and a SEM-EDS to identify target phases. It was then gold-coated and loaded into NanoSIMS 50 (AORI, UTokyo) to conduct U–Pb dating of phosphates (apatite, merrillite) and ²⁰⁷Pb–²⁰⁶Pb dating of surrounding silicate phases and baddeleyite. The previously established measurement protocols and an age-reference apatite were utilized [3,4]. After NanoSIMS dating, the mount was repolished to remove the gold-coat. Detailed mineralogical observations were undertaken using a FE-SEM-FIB (Helios G4 UC at N-BARD, Hiroshima) and the elemental composition analyses were conducted by EPMA (JXA-iSP100 at N-BARD, Hiroshima). Crystal orientations and internal microstructures of the phosphates were examined by EBSD using a ZEISS Crossbeam 550 SEM equipped with an Oxford Instruments Symmetry 2 EBSD detector (Open Univ.). The analytical conditions and data processing protocols followed the previous methods [5,6]. Crystallinity of the plagioclase was also examined by a TEM observation (JEM-F200 at N-BARD, Hiroshima) of an ultra-thin section. Trace element compositions of the powdered bulk sample of NWA 16895 was measured using an ICP-MS (Agilent 7700x at Kochi, JAMSTEC) after acid digestion and column chemistry.

Results & Discussion: As previously reported [1,2], the whole rock mineralogy of NWA 16895 (Fig. 1a) is mainly composed of zoned pyroxenes (pigeonite and augite) intergrown with needle-like plagioclase and ilmenite. Minor phases include Fe-rich olivine, K-feldspar, silica, troilite, apatite, merrillite, and baddeleyite. Symplectite structures of fayalitic olivine and K-Al-rich silica spherules, along with elongated apatite, often occur at the rim of pigeonite (Fig. 1b–c). A small pocket of impact melt glass was also observed. There are rare calcite veins, suggesting a small degree of terrestrial weathering.

The compositions of pyroxenes vary from a Fe/Mg augite core to Fe-rich pigeonite rim (Fig. 2a). Their Fe/Mn ratios are \sim 70–80, consistent with typical lunar samples. Ti# and Fe# of the pyroxenes show a broad agreement with the lunar low-Ti basalt to very low-Ti basalt compositions. The plagioclase has bytownite to anorthite compositions and often co-exists with K-feldspar (Fig. 2b). The apatite is rich in F, Fe, Si but poor in Cl (i.e., fluorapatite). The co-existing merrillite presents very high concentrations of rare earth elements (up to \sim 3 wt.% for Ce₂O₃).

The band contrast and inverse pole figure maps of some phosphates grains present single orientations with little internal grain misorientations, suggesting they have not recorded major impact deformation. On the other hand, the preliminary TEM observation indicates the plagioclase was converted into amorphous (i.e., maskelynite) during an impact with pressures at ~15–20 GPa [7].

The $^{207}\text{Pb}-^{206}\text{Pb}$ isochron age is determined from the NanoSIMS measurements on the phosphates, baddeleyite, impact melt glass, silica, fayalite, and plagioclase at 2006 ± 540 Ma (MSWD = 1.0; Fig. 3). The large uncertainty is due to the relatively scattered $^{207}\text{Pb}/^{206}\text{Pb}$ ratios at around the y-intercept (Fig. 3). The slope of the $^{207}\text{Pb}-^{206}\text{Pb}$ isochron infers highly radiogenic initial Pb composition for this meteorite, corresponding to the source μ -value up to ~ 2000 (Fig. 3). Meanwhile, the U–Pb isochron of the phosphates (without other phases) presents a somewhat older age of ~ 2.7 Ga for some reason.

The textural and compositional features of NWA 16895 show more similarities to lunar basalts rather than martian augite basalts. Surprisingly, the sample appears similar to Chang'e-5 returned samples from Oceanus Procellarum terrain [8]. The two-billion-year-old Pb–Pb age is broadly consistent with the Chang'e-5 lunar basalts (2030 \pm 4 Ma; [8]) and younger than Chang'e-6 basaltic samples collected from the lunar far-side (2807 \pm 3 Ma; [9]), although the large error of our isochron (\sim 500 Ma) makes interpretations difficult. The high abundances of rare earth elements and the high μ -value of \sim 2000 indicates NWA 16895 is a member of lunar KREEP-rich basalt, with potentially, the youngest age. The apparently intact crystal orientations of the phosphates support an interpretation of its igneous origin at \sim 2 Ga. In contrast, the presence of maskelynite, as well as the impact melted glass, suggests an impact metamorphism to some extent. Ther is also a possibility that NWA 16895 was originally formed much earlier and was reheated at \sim 2 Ga due to an impact. Moreover, the relationship between the symplectic fayalite-silica and the apatite remains unclear and would be highly complicated. Further study on its mineralogy, geochemistry, oxygen isotopic compositions and chronology will be helpful to establish a solid interpretation concerning the origin and provenance of this meteorite.

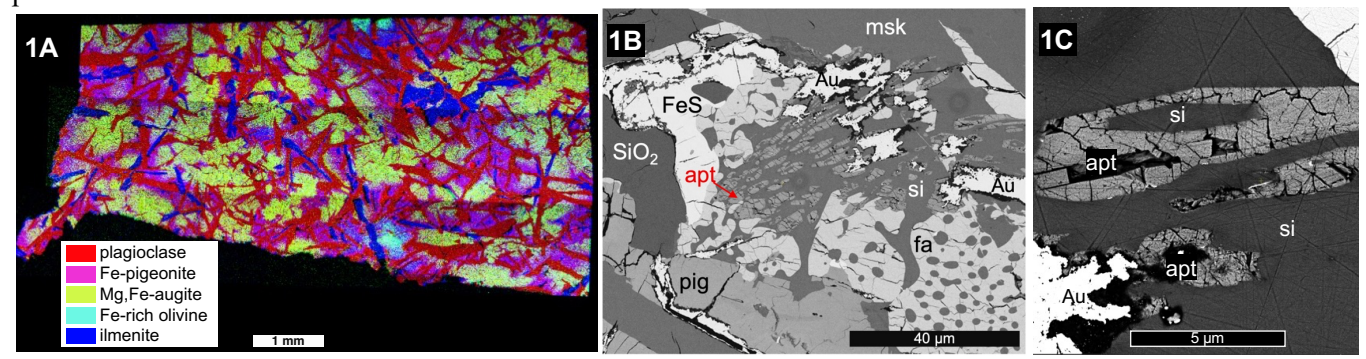


Fig. 1. (A) The EDS color map of the studied sample. (B, C) the BSE images of the symplectite with fayalite (fa), K-Al-rich silica (si) and apatite (apt), adjacent to pigeonite (pig) and maskelynite (msk). (Au: remaining gold coating)

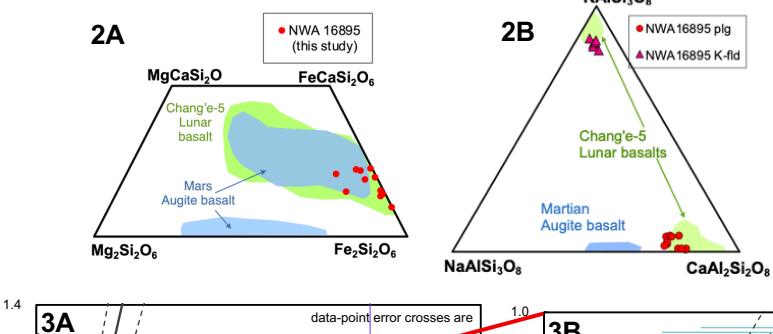


Fig. 2. Compositional diagrams. (A) the Ca-Mg-Fe plot of pyroxenes and (B) the K-Na-Ca plot of feldspars. Literature data of the same meteorite [1], lunar samples [8,9], and martian augite basalt [10] are shown as shadows.

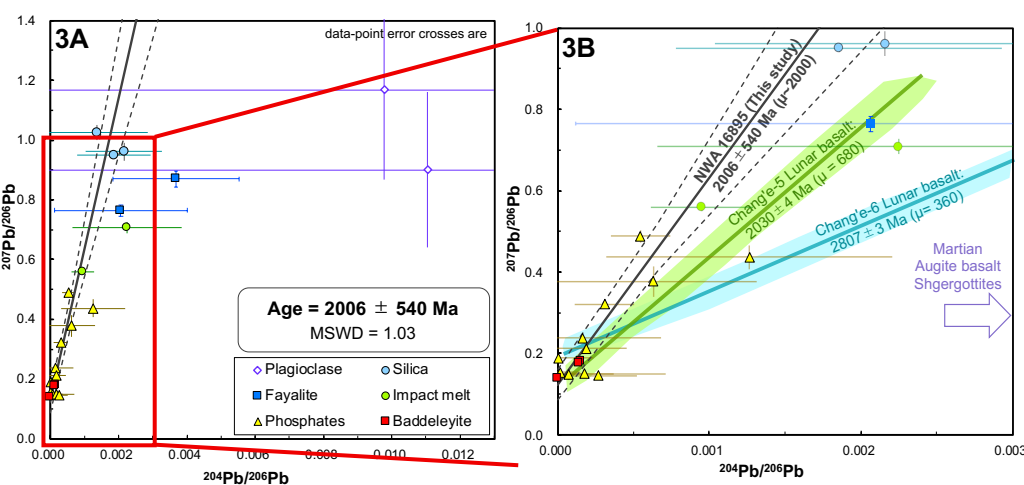


Fig. 3. (A) Pb isotope data of phosphates, baddeleyite, impact melt glass, silica, favalite, and plagioclase. A11 define the Pb-Pb isochron age at 2006 ± 540 Ma with the high source μvalue of ~ 2000 . (B) The enlarged plot of rectangle in A. Literature isochrons for the lunar samples [8,9] are shown as shadows.

References: [1] Driscoll, E. and Herd, C. D. K. (2025) 56th LPSC, Abstract #2356. [2] Koike, M. et al. (2025) 87th MetSoc, Abstract #5193. [3] Koike, M. et al. (2020) *EPSL* 549, 116497. [4] Sano, Y. et al. (1999) *Chem. Geol.* 153, 249–258. [5] Rider-Stokes, B. G. et al. (2023) *Nature Astron.* 7, 836–842. [6] Rider-Stokes, B. G. et al. (2024) *MaPS* 59, 23–29. [7] Hu, J. et al. (2023) *Sci. Adv.* 9, eadf2906. [8] Li, Q-L. et al. (2021) *Nature* 600, 54–60. [9] Zhang, W.W.L. et al. (2024) *Nature* 643, 356–360. [10] Herd, C.D.K. et al. (2023) *MaPS* 58, 158–164.

Mineralogical Study of Characteristic Microstructure Formed at the Late Crystallization Stages of Basaltic Shergottites

Shingo Fujioka¹, Takashi Mikouchi^{1,2}, Sojiro Yamazaki¹, Wataru Satake³ and Akira Yamaguchi⁴

¹Dept. Earth and Planetary Sci., Univ. of Tokyo, Hongo, Tokyo 113-0033, Japan

²Univ. Museum, Univ. of Tokyo, Hongo, Tokyo 113-0033, Japan

³Inst. Geo-Cosmology, Chiba Inst. Tech., Narashino, Chiba 275-0016, Japan

⁴National Institute of Polar Research (NIPR), Tachikawa, Tokyo 190-0014, Japan

Introduction: Basaltic shergottites are mainly composed of pyroxene and maskelynite and show a higher degree of magmatic differentiation than other shergottite groups [e.g., 1]. Consequently, in some samples, the pyroxene is remarkably iron-rich, and a fine-grained, three-phase or two-phase symplectite texture is observed, consisting of fine-grained fayalite + silica mineral ± hedenbergite [e.g., 2]. These mineral assemblages are interpreted to be breakdown products of pyroxferroite [e.g., 3]. Additionally, some maskelynite partly contain an intergrowth texture of K-feldspar-rich glass and a silica mineral, which is thought to be the result of feldspar differentiation upon crystallization [e.g., 4]. However, few studies have comprehensively investigated such pyroxene symplectites and feldspar differentiation textures in basaltic shergottites. Therefore, in this study, we categorized eight basaltic shergottite samples, including those recently discovered in the Sahara, based on the presence or absence of these two distinctive late-stage crystallization textures, and compared their chemical compositions and redox states to examine differences in the magmatic crystallization processes on Mars.

Samples and analytical methods: In this study, thin section samples of NWA 2975, 6963, 12965, 13327, 13716, 14607, 15016, and Los Angeles were used. After detailed observation with an optical microscope and a Field Emission Scanning Electron Microscope (FE-SEM) (JEOL JSM-7000F at Univ. of Tokyo), mineral compositions were analyzed using a Field Emission Electron Probe Microanalyzer (FE-EPMA) (JEOL JXA-8530F at Univ. of Tokyo) and an Electron Probe Microanalyzer (EPMA) (JEOL JXA-8200 at NIPR). Furthermore, the valence state of iron in maskelynite was measured by Fe-XANES (at the Photon Factory beamline BL-4A of the High Energy Accelerator Research Organization, KEK) to compare their redox states.

Results: After the petrographic observations and mineral compositional analyses, we found that the samples analyzed in this study were classified into three types:(a) samples containing both pyroxene symplectite and feldspar differentiation textures, (b) samples lacking pyroxene symplectite but containing feldspar differentiation textures, and (c) a sample lacking both pyroxene symplectite and feldspar differentiation textures. The type (a) includes NWA 14607 and Los Angeles, in which the pyroxene is more iron-rich than in (b) and (c), with compositions of En₅₋₅₅Wo₁₁₋₃₈ (Fig. 1). The type (b) includes NWA 2975, 6963, 12965, 13327, and 15016, with pyroxene compositions of En₂₀₋₆₀Wo₄₋₄₀ (Fig. 1) NWA 13716 was the only sample belonging to the type (c), with the most magnesian pyroxene composition of En₃₀₋₆₀Wo₁₁₋₃₄ (Fig. 1)

A correlation between pyroxene composition and the maskelynite composition was found. The maskelynite in (c) NWA 13716 is $An_{66-57}Or_{0-1}$, which is richer in Ca and poorer in K than those in (a) and (b) $(An_{59-44}Or_{1-9})$ (Fig. 2). The K-feldspar-rich glass forming the feldspar differentiation textures was diverse; some like Los Angeles, NWA 2975 and NWA 6963 exhibit wide compositional ranges (Los Angeles: $Na_2O = 2-4$ wt% $K_2O = 4-7$ wt%, NWA 2975: $Na_2O = 2-5$ wt% $K_2O = 1-4$ wt%,: $Na_2O = 2-4$ wt% $K_2O = 0.5-8$ wt%), while NWA 14607 exhibits a relatively narrow compositional range ($Na_2O = 4-6$ wt% $K_2O = 2-3$ wt%) (Fig. 3). The proportion of ferric iron to the total iron ($Fe^{3+}/\Sigma Fe$) in maskelynite was 0.11-0.12 for (a) NWA 14607, 0.23-0.27 for (b) NWA 13327, and 0.12-0.16 for (c) NWA 13716, respectively.

Although it is noted that the three-phase symplectite in Los Angeles is often in contact with the mesostasis [2], in the type (a) samples of this study, two-phase symplectite textures were frequently found adjacent to feldspar differentiation textures. Unlike Los Angeles, three-phase symplectite in NWA 14607 was observed independently, not in contact with Ca-Fe pyroxene.

Discussion and Conclusion: This study, through the analysis of multiple basaltic shergottites, has shown that the degree of magmatic crystallization of pyroxene and maskelynite corresponds to the presence or absence of the forementioned late-stage crystallization textures. In other words, the pyroxene in the type (a) samples is more ironrich and the maskelynite has a lower Ca content than in types (b) and (c), which corresponds to a more advanced stage of crystal differentiation in samples possessing more diverse late-stage textures. It is also suggested that the

degree of pyroxene accumulation was not so advanced to drastically change the crystallizing plagioclase compositions in these samples although some samples are clearly pyroxene dominant over maskelynite. While the two type (a) samples exhibit similar late-stage crystallization textures, they differ in the morphology and mineral modes of their pyroxene and maskelynite.

Since all analyzed samples are chemically "enriched", the relationship between the presence or absence of late-stage crystallization textures and characteristics such as light rare earth element (LREE) compositions remains unclear. Similarly, no clear correlation was observed between the presence of these late crystallization stage textures and the composition of the K-feldspar-rich glass or the redox state of the maskelynite. Probably, the redox states do not play an important role for the formation of these textures since they are widely observed in Martian, lunar and Vesta samples [e.g., 5,6]

In the future, a comprehensive investigation will be necessary, considering this perspective for other samples and further examining whether these textures formed concurrently with crystallization or through secondary decomposition.

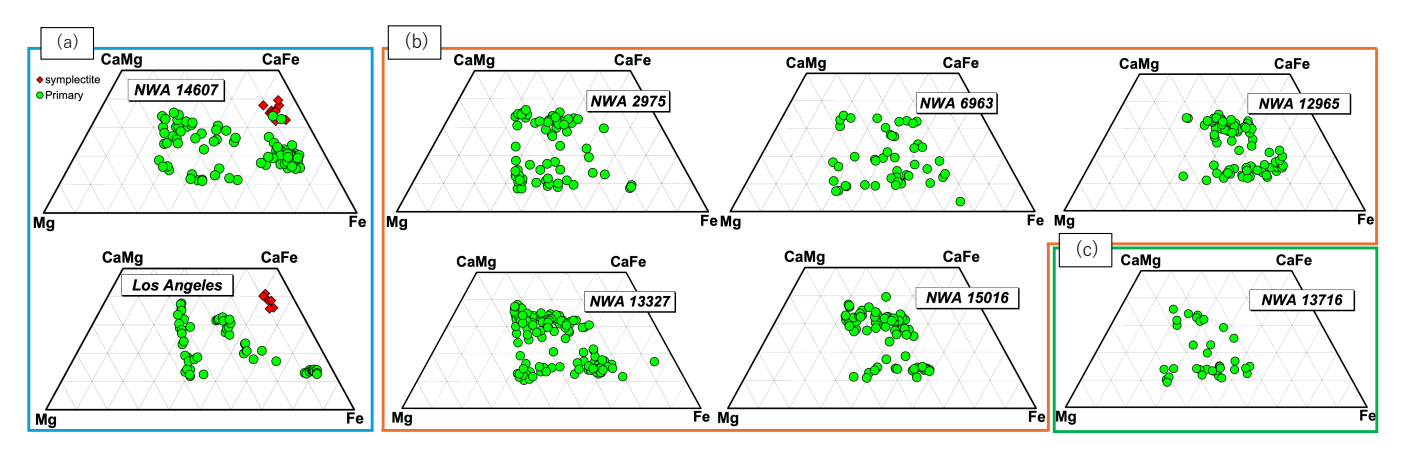


Fig. 1. The pyroxene compositions of each basaltic shergottites on the pyroxene quadrilateral. Red diamonds are hedenbergite forming symplectite.

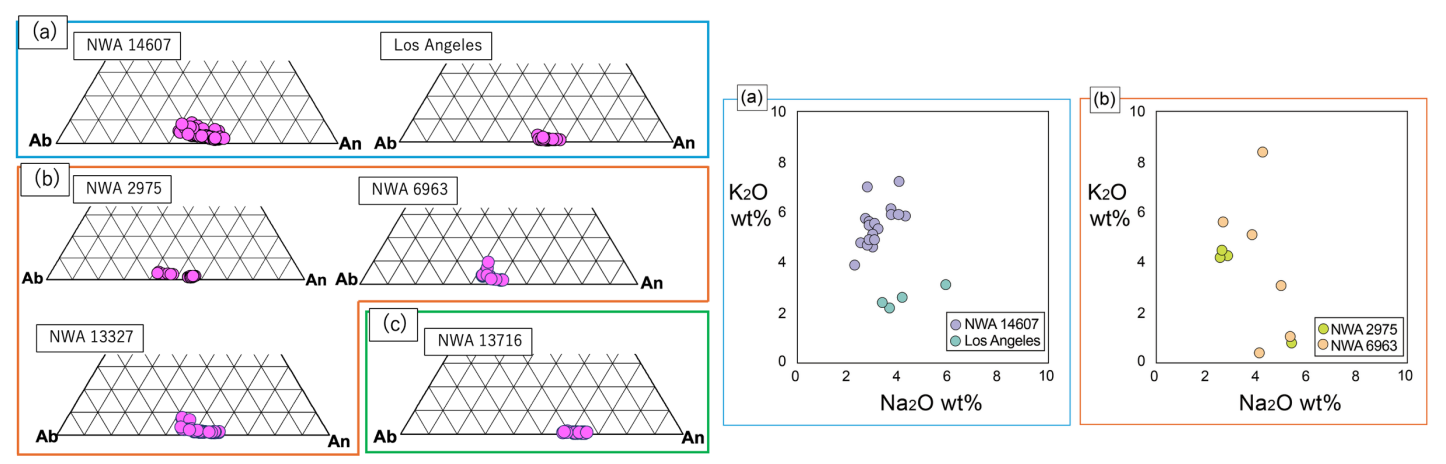


Fig. 2. The maskelynite compositions of each basaltic shergottites on the Ca-Na-K ternary diagram.

Fig. 3. Na-K variations of the K-feldspar-rich glass found in types (a) and (b) samples.

References:

[1] Udry A. et al. (2020) Journal of Geophys. Res.: Planets, 125, e2020JE006523. [2] Aramovich C. J. et al. (2002) American Mineral., 87, 1351-1359. [3] Rost D. et al. (2009) Meteorit. Planet. Sci., 44, 1225-1237 [4] Lindner M. et al. (2022) Meteorit. Planet. Sci., 57, 2017-2041. [5] Patzer A. et al. (2012) Meteorit. Planet. Sci., 47, 1475-1490. [6] Fagan T. J. et al. (2003) Meteorit. Planet. Sci., 38, 529-554.

Chemical composition and shock conditions for low-temperature transformation of Fe-Cr-Ti spinel to its high-pressure phases in Martian meteorites

Atsushi Takenouchi¹, Yohei Igami², Akira Miyake², Takashi Mikouchi³, Akira Yamaguchi⁴

¹The Kyoto University Museum, Kyoto University, ²Graduate school of Science, Kyoto University,

³The University Museum, The University of Tokyo, ⁴National Institute of Polar Research

Research on high-pressure minerals is crucial for understanding shock metamorphism and constraining the state of Earth's deep interior. Numerous high-pressure phases have been identified in meteorites. In this study, we focus on the phase transitions of the chromite—ulvöspinel solid solution, which is widely distributed in meteorites. Chromite exhibits two distinct high-pressure polymorphs above ~16–18 GPa: xieite (space group *Cmcm*), which is stable above ~1300 °C, and chemmingite (space group *Pnma*), which is stable below ~1300 °C (Ma et al. 2019). Both minerals represent typical high-pressure and high-temperature phases found near shock-melt regions in Martian meteorites. By contrast, ulvöspinel has only one high-pressure phase, tschaunerite (space group *Cmcm*), stable above ~16 GPa (Ma et al. 2025). Notably, a *Pnma*-type phase analogous to chemmingite has not been predicted for ulvöspinel. In our previous work, we showed that innumerable lamellae of chemmingite form within chromite even under relatively low-temperature conditions, away from melt veins in Martian meteorites, and that this transition is facilitated in Ti-rich compositions. These observations suggest that high-pressure phase transitions in the chromite—ulvöspinel solid solution are highly sensitive to both composition and shock metamorphic conditions. Therefore, identifying the types of high-pressure phases and the conditions of their formation provides important constraints on shock metamorphism. For this reason, this study investigates the relationship between composition and high-pressure phases in Cr–Ti spinels from Martian meteorites.

This study examines several Martian meteorites that record varying degrees of shock metamorphism, with the aims of identifying high-pressure phases and evaluating their compositional dependencies. We prepared seven thin sections of Martian meteorites; Asuka (A) 12325, Northwest Africa (NWA) 12241, NWA 13366 (poikilitic), Amgala 001 (olivine-phyric), NWA 10703, NWA 16127 and Swayyah 002 (basaltic). Most of these meteorites have preiously been studied and their high-pressure phases were reported in detail (Takenouchi et al. 2025). Observations and compositional analyses were carried out using scanning electron microscopy with energy-dispersive X-ray spectroscopy (SEM–EDS, JEOL JSM-7001F), specimen preparation by focused ion beam (FIB, Helios NanoLab G3 CX), and transmission electron microscopy (TEM, JEM-2100F) at the Graduate School of Science, Kyoto University. Beam current measurements for Quantitative EDS analyses were performed using Co as the standard. When the measured stoichiometry did not correspond to that of a spinel, FeO was progressively converted to Fe₂O₃ to adjust the stoichiometry and enable calculation of Fe³⁺ content. Spinel compositions are treated as a solid solution among FeCr₂O₄ (chromite, Chr) – MgAl₂O₄ (spinel, Sp) – Fe₂TiO₄ (ulvöspinel, Ulv) – Fe²⁺Fe³⁺₂O₄ (magnetite, Mag). The compositions of Chr#, Sp#, Mag# are defined as Chr#, Sp#, Mag# = (Cr, Al, Fe³⁺)/ (Cr + Al + 2Ti + Fe³⁺), while Ulv# is defined as 2Ti / (Cr + Al + 2Ti + Fe³⁺).

The compositional ranges of spinel obtained by our SEM-EDS analysis are summarized in Table1. Spinel in poikilitic shergottites exhibits various Ti contents, with most grains classified as chromite. Two spinel grains in A12325 are classified as ulvöspinel containing high Cr abundances. These Cr-rich ulvöspinels display lamellar textures resembling the chenmingite lamellae observed in Ti-rich chromite. Our FIB-TEM analyses further revealed that selected-area electron diffraction patterns from the lamellae in Cr-rich ulvöspinel can be indexed as the chenmingite-type structure (*Pnma*), indicating the presence of *Pnma*-type high-pressure phase of ulvöspinel. Spinel in Amgala 001 exhibits pronounced chemical zoning, with Cr-rich cores and Ti-rich rims. The Ti-rich rims contain fine ilmenite lamellae produced by igneous exsolution. In addition, spinel from Amgala 001 shows chenmingite lamellar textures in both Cr-rich and Ti-rich chromite region. By contrast, spinels in the three basaltic shergottites consists exclusively of ulvöspinel with limited compositional variations and low Cr contents. No chenmingite-like lamellar textures were observed in these Cr-poor ulvöspinels.

All of the shergottites studied exhibit shock metamorphic textures. As previously reported, A 12325 and NWA 12241 contain partially vitrified plagioclase, indicating relatively weak shock pressures of around 17-22 GPa, whereas the other shergottites contain completely vitrified plagioclase (maskelynite). Although spinels in A 12325 have chemical compositions similar to those in NWA 12241, they contain much more abundant chemingite

lamellae. NWA 13366 contains brown-colored olivine, consistent with severe shock metamorphism at ~55 GPa (Takenouchi et al. 2018). Amgala 001 and Swayyah 002 contain thin shock-melt veins, and their pyroxene exhibit mosaicism, indicative of shock pressures exceeding ~30 GPa. NWA 16127 and NWA 10703 contain abundant shock-induced melt, and their plagioclase transformed into normal glass due to high-temperatures, suggesting peak shock pressure of >45 GPa. In NWA 16127, revitrification of maskelynite along grain boundaries of surrounding minerals is observed.

Our observations are summarized in Figure 1, which shows the relationship between the estimated shock pressures and Ulv# of spinel with/without chenmingite lamellae. Chenmingite can form from chromite even away from shock-melt at around 30 GPa, and the required pressure decreases with increasing Ti contents in chromite. Ulvöspinel, by contrast, rarely transforms into its high-pressure phase regardless of shock pressure, suggesting that transformation of ulvöspinel to tschaunerite must need high-temperature. However, elevated Cr contents may facilitate the transform of ulvöspinel into chenmingite-like phase at relatively low pressure ~20 GPa without high-temperature. In contrast, chenmingite lamellae are absent in severely shocked meteorites, regardless of Ulv#. This may reflect the effects of high shock temperatures, which either inhibit the transformation to low-temperature phases or promote the back-transformation. Thus, chenmingite lamellae could serve as a useful indicator of shock pressure around 17~30 GPa under relatively low-temperature conditions. We will further investigate the stability of chenmingite lamellae at high temperatures to better constrain both their formation and erasure conditions.

Table 1 Compositional ranges of Fe-Cr-Ti spinel in Martian m	meteorites st	udied
--	---------------	-------

1	0									
	Type	N. of	Cr-rich spinel			Ti-rich spinel				
		data	Chr#	Ulv#	Sp#	Mag#	Chr#	Ulv#	Sp#	Mag#
Asuka 12325	poikilitic	154	81.2	2.4	12.3	3.5	22.9	56.9	7.3	13.0
NWA 12241	poikilitic	48	78.8	3.6	14.0	0.9	31.7	49.0	10.7	7.8
NWA 13366	poikilitic	141	84.5	2.1	10.7	2.3	33.8	49.0	9.6	7.5
Amgala 001	ol-phyric	107	80.8	2.0	13.1	3.7	0.8	79.5	5.4	14.0
NWA 16127	basaltic	7	0.3	73.2	4.3	19.0	0.2	77.7	4.3	17.7
Swayyah 002	basaltic	30	8.8	61.9	14.8	13.6	3.3	76.1	3.8	16.7
NWA 10703	basaltic	18	2.2	75.0	4.0	18.9	0.6	77.2	3.5	18.3

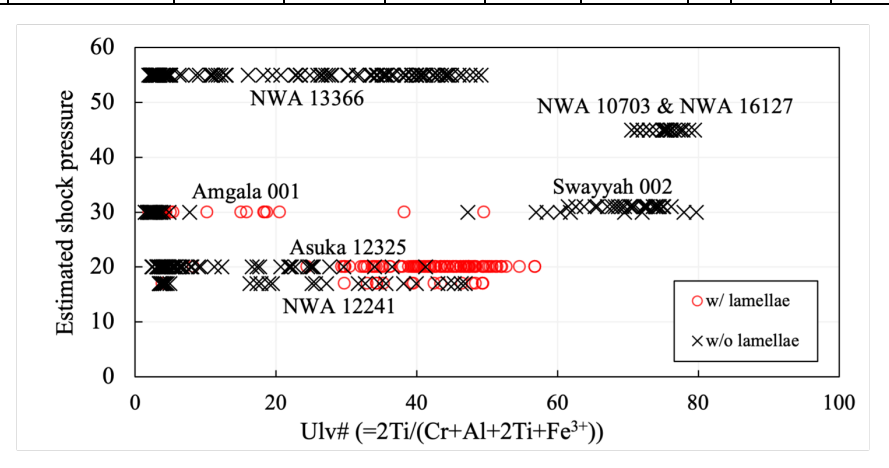


Figure 1 Ulvöspinel contents and estimated shock pressure in spinel with and without lamellae.

- Ma C., Tschauner O., Beckett J. R., Liu Y., Greenberg E., and Prakapenka V. B. 2019. Chenmingite, FeCr₂O₄ in the CaFe₂O₄-type structure, a shock-induced, high-pressure mineral in the Tissint martian meteorite. *American Mineralogist* 104:1521–1525.
- Ma C., Tschauner O., Beckett J. R., and Prakapenka V. B. 2025. New high-pressure Fe-Ti oxide minerals in the Shergotty Martian meteorite: Feiite, Fe²⁺₂(Fe²⁺Ti⁴⁺)O₅, liuite, FeTiO₃, and tschaunerite, (Fe²⁺)(Fe²⁺Ti⁴⁺)O₄. *Meteoritics and Planetary Science* 60:375–391.
- Takenouchi A., Mikouchi T., and Yamaguchi A. 2018. Shock veins and brown olivine in Martian meteorites: Implications for their shock pressure–temperature histories. *Meteoritics and Planetary Science* 53.
- Takenouchi A., Igami Y., Miyake A., Mikouchi T., and Yamaguchi A., Relation between chemingite distribution and composition of Cr-Ti spinel in Martian meteorites, 87th Annual Meeting of the Meteoriteical Society abst, #5154 (LPI contrib. No. 3088), 2025.

An aerial drone equipped with a hyperspectral imaging system: Application to Greenland and Antarctica meteorite survey

Levente Tóth¹ and Arnold Gucsik²

¹John Neumann University, Kecskemét, Hungary

²Eszterházy Károly Catholic University, Eger, Hungary

Unlike traditional cameras that capture light in three broad bands (red, green, and blue), a hyperspectral sensor divides the electromagnetic spectrum into a vast number of very narrow, contiguous bands. This process creates a hyperspectral data cube, a three-dimensional dataset where two dimensions represent spatial information (x, y) and the third dimension represents the spectral information (λ, y) or wavelength). Every pixel in the data cube contains a full spectrum, providing a detailed "fingerprint" of the material at that specific location.

This is especially useful for geological and mineralogical studies because most minerals have distinct absorption and reflection features at specific wavelengths. These unique spectral signatures are used to identify and map materials. For example, iron-rich minerals, which are common in many types of meteorites, show characteristic absorption features in the visible and near-infrared (VNIR) to short-wave infrared (SWIR) ranges of the spectrum. By analyzing the spectral data, researchers can automatically classify and map the locations of these target minerals.

The vast, largely uninhabited ice sheets of Greenland and Antarctica are ideal for meteorite hunting because the stark white background makes dark, extraterrestrial rocks stand out. However, the sheer scale of the area and the harsh environment make ground-based searches logistically difficult and timeconsuming. A drone-based hyperspectral system overcomes these challenges by offering a rapid, nondestructive, and highly efficient survey method.

A typical mission would involve pre-programming a drone to fly a precise "push-broom" scanning pattern over a designated search area. The hyperspectral sensor captures data line by line as the drone moves, building up the data cube of the landscape below. Once the data is collected, it is processed and analyzed using specialized software. Algorithms are used to match the spectral signatures of each pixel to a library of known meteorite and terrestrial rock spectra. This process allows for the rapid identification of potential meteorite candidates, which can then be flagged for a follow-up ground inspection.

Despite its advantages, operating a drone in Greenland and Antarctica presents significant challenges. The extreme cold can reduce battery life and affect the performance of electronic components. High winds and icing are also major risks, potentially causing a crash or affecting the drone's flight stability, which is crucial for accurate push-broom scanning. Furthermore, the limited GPS signal near the magnetic poles can affect navigation and precise positioning. Specialized, ruggedized drones and sensors are required to withstand these conditions.

In conclusion, the integration of hyperspectral imaging with drone technology provides an unprecedented level of efficiency and accuracy for meteorite searches in remote polar regions. By leveraging the unique spectral signatures of meteorites, this system enables the rapid and precise identification of targets that would be difficult or impossible to find with traditional methods. While logistical challenges remain, the technology represents a significant leap forward in the field of planetary science and exploration.

Asteroids - Do Look Up! - A school's outreach project using Arctic and Antarctic micrometeorites and meteor cameras.

<u>Richard C. Greenwood¹</u>, Sara S. Russell², Liam Perara³, Ashley J. King², Alice Dunford¹, Martin D. Suttle¹, Sharif Ahmed³, Mahesh Anand¹, Motoo Ito⁴, James Malley¹ Marissa Davis⁵

¹The Open University, UK. ²The Natural History Museum, UK. ³Diamond Light Source, UK. ⁴Kochi Institute (JAMSTEC), Japan. ⁵The Griffin Schools Trust, UK. EMAIL: richard.c.greenwood@open.ac.uk

Introduction: "Asteroids – Do Look Up!" is a two-year science project funded by the UK's Science and Technology Facilities Council (STFC) that started activities in August 2024. The project is aimed at students aged 7 to 14. During the initial year of activity 13 schools, located in the Southeast and Midlands regions of England, participated in the project. Students attending these schools are generally from relatively disadvantaged social backgrounds. The aim of the project is to use space science to inspire these students and increase their "science capital".

Motivation: As highlighted by the King's College, London ASPIRES report (Archer Ker et al., 2013), there is widespread concern that young people are not sufficiently motivated to study STEM subjects after the age of 16. In addition, the background of those who do choose to follow a STEM curriculum can be narrow, with women, some ethnic minorities, and economically disadvantaged groups, significantly underrepresented. The ASPIRES study found that only 15% of students surveyed intended to follow a scientific career. One of the main conclusions of the report was that: "Efforts to broaden students' aspirations, particularly in relation to STEM, need to begin at primary school." One way to improve STEM subject uptake is by providing inspirational outreach partnerships with schools. In particular, there is evidence that space-related activities are effective at raising students interest in STEM subjects (Rosu and Ceobanu, 2022). The motivation behind Asteroids – Do Look Up! was to raise the science capital of the target group by introducing them to a range of inspirational space-related activities.

Proposed methodology: A number of distinct activities were planned as part of the project. In a classroom setting, students would use both digital microscopes and portable scanning electron microscopes (SEM) to study extraterrestrial materials, including Antarctic and Arctic micrometeorite-bearing sediments. By dissolving and filtering Permian halite sediments, students would attempt to concentrate extraterrestrial material. Micrometeorite searches were planned in areas close to the schools, following the methods of Suttle et al. (2021). Each school would be given a dedicated meteor camera, providing daily feedback on local meteor activity. These cameras would be part of the Global Meteor Network (Roggemans et al., 2024). Extraterrestrial material located by the students would be imaged by SEM techniques at the Open University and the most promising particles selected for analysis on the Dual Imaging And Diffraction (DIAD) beamline at the Diamond Light Source synchrotron facility. Images obtained at the Open University and on DIAD would be provided to the students who had located the relevant particles. In this way, a firm link would be made between classroom activities and the more sophisticated methodologies employed at facilities such as DIAD. Evaluation by an outside team of science auditors would be an integral part of the project. Year one activities: During the first year of the project the emphasis has been on visiting schools and undertaking classroom micrometeorite collection activities. We were fortunate to have micrometeorite-rich materials collected in Antarctica and a particularly large sample of micrometeorite-bearing cryoconite collected in Greenland in the early 1990s. Each school in the project has been visited twice. During the first round of school visit students were introduced to meteorites and micrometeorites using the Open University's outreach collection. This is a resource that contains a selection of hand specimens covering the full range of meteorite types. The second visit to the schools involved workshops in which the students used digital microscopes (Fig. 1) to hunt for micrometeorites in Arctic and Antarctic sediments. Permian salt was also dissolved and filtered with the aim of locating extraterrestrial material. The classroom workshops were linked to the UK National Curriculum (KS2) which specifies that students need to have hands on experience of separating mixtures. The laboratory work on micrometeorites has been a particularly successful aspect of the project so far. Extraterrestrial particles were located during the majority of school visits and this material is currently being imaged at the Open University. At a number of the schools, sediments were collected from classroom roofs (Fig 1 left). However, due to time constraints, and health and safety considerations, this aspect of the project has not yet been fully implemented. This will be a focus of the project in Year Two.



Fig. 1 (Left) Collecting sediment from a classroom roof. (Centre) Digital microscope with micrometeorites collected from Greenland cryoconite sediment. (Right) Students using a digital microscope to study micrometeorites.

Teating of micrometeorite particles to refine analytical protocols has been successfully carried out at DIAD (Fig. 2) and analysis of student located material will commence shortly. During Year One meteor camera components were sourced and two prototype cameras constructed. A third fully operational camera was obtained from Istrastream in Croatia. Once a number of remaining logistical issues are resolved, these cameras will be installed in schools early in Year Two. Further cameras will be constructed once the prototypes have been fully tested.

Planned activities for Year Two: Based on the experience gained during Year One, there will be a change in emphasis to the activities conducted in Year Two. Discussion with the Griffin Schools Trust science leads highlighted the need for additional time to complete the various activities. Consequently, in Year Two school visits will be of longer duration with students taken off timetable for a morning or afternoon. Additional micrometeorite searches will be conducted by technical staff at the schools with some student participation, as constrained by health and safety considerations. Analytical data and images collected at the Open University and DIAD on particles located during Year One will be fed back to the respective schools.

Evaluation: Formal evaluation of the project, with the assistance of outside assessors, is ongoing. The project made good progress in its first year, with positive feedback from students and teachers. The classroom-based activities worked well. A range of challenges has meant that local micrometeorite searches were not implemented in the manner originally envisaged. The meteor cameras are making progress, albeit at a slower pace than we would have hoped. However, we are optimistic that significant progress towards the aims of the project will be achieved in Year Two.

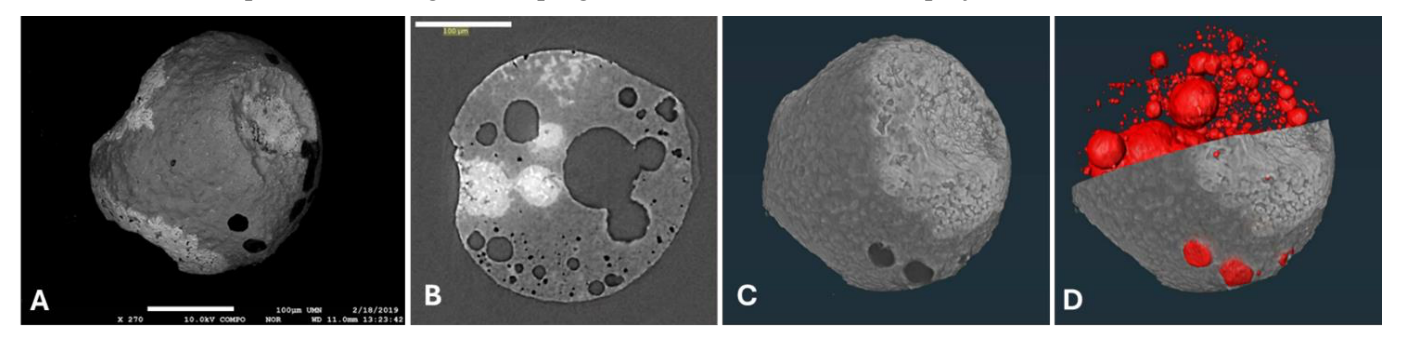


Fig. 2 (A) SEM image of micrometeorite, (B) Reconstructed XY slice from DIAD tomography through the same micrometeorite, (C) Rendered 3D volume of the surface of the scanned micrometeorite, (D) Visualisation of porosity in micrometeorite.

References

Archer Ker L. et al., (2013) https://kclpure.kcl.ac.uk/ws/portalfiles/portal/64130521/ASPIRES_Report_2013.pdf
Rosu D. and Ceobanu C. (2022) ERD 2022..10.15405/epes.23056.58; Suttle MD, Hasse T, Hecht L. (2021) MAPS 56, 1531-1555. Roggemans P. et al. (2024) https://www.emeteornews.net, vol. 10, no. 2, p.67-101.

Mt. Oikeyama as the first probable impact structure in Japan: Revisited

<u>Arnold Gucsik</u> Eszterházy Károly Catholic University, Eger, Hungary

Mount Oikeyama, a prominent geological feature in Nagano Prefecture, Japan, has been proposed as the country's first confirmed impact crater. This hypothesis challenges traditional geological interpretations of the region and presents a compelling narrative of a significant cosmic event that impacted the Japanese archipelago. The unique morphology of Mt. Oikeyama, combined with geochemical anomalies and geophysical data, points towards an extraterrestrial origin (Sakamoto et al., 2010). Furthermore, considering the scenario of an impact during the Last Glacial Maximum (Ice Age), when parts of Japan, including mountainous regions, experienced colder temperatures and potentially harbored ice sheets or extensive permafrost, introduces an intriguing possibility of an ice-target impact event.

Mt. Oikeyama is located on the Shirabiso Highland in the Southern Japanese Alps (Akaishi Mountains) in Nagano Prefecture, Japan. The regional geology of this area is dominated by the Chichibu Paleozoic terrain, an accretionary complex formed over millions of years as oceanic plates were subducted beneath the Eurasian plate. The bedrock consists mainly of Mesozoic and Paleozoic sandstones, mudstones, and cherts, which serve as the host rocks in which shock-metamorphic features have been identified.

The primary evidence supporting Mt. Oikeyama's impact origin stems from its distinct circular morphology, which stands in stark contrast to the typical volcanic or tectonic landforms of the Japanese islands. The feature exhibits a central uplift, a defining characteristic of complex impact craters, surrounded by a depression that may represent the crater rim. The estimated diameter of the crater is approximately 1.2 kilometers.

Geochemical and mineralogical studies have further bolstered the impact hypothesis. Analyses of rocks within and around Mt. Oikeyama have revealed the presence of shocked quartz mineral grains exhibiting microscopic planar deformation features (PDFs). Researchers have used techniques like Micro-Raman spectroscopy to confirm these anomalous structures, which form under immense pressures and temperatures far exceeding those found in typical geological processes (Sakamoto et al., 2010; Okumura et al., 2012). The existence of these PDFs is considered unequivocal evidence of a hypervelocity impact. The age of the Mt. Oikeyama impact structure is currently unknown. It is presumed to be relatively old due to the heavy erosion, but a precise radiometric age has not yet been determined, making it difficult to link the impact to a specific geological or climatic event.

The Last Glacial Maximum (LGM), roughly 26,500 to 19,000 years ago, was a period of significantly colder global temperatures, leading to the expansion of ice sheets and glaciers. If the impact event occurred during this period, the colliding body would have struck an ice-rich target, a scenario that has profound implications for crater formation and preservation. An impact into a layered target of ice and rock would differ significantly from one into solid rock.

A modeling scenario for such an event would unfold as follows: a shock wave first hits the sandstone layer, compressing and fracturing the rock and creating the shocked quartz seen today. As the wave penetrates the underlying ice, the ice's lower density and strength would cause a massive, energetic vaporization, creating a superheated steam plume. This would result in a crater that is wider and shallower than a crater formed in a purely rocky target of the same energy (Melosh, 1989). Post-impact, the eventual melting of the ice target would have led to significant collapse and modification of the crater structure, which would help to explain why the Mt. Oikeyama structure is so heavily eroded and subtle today. While direct evidence for this specific scenario at Mt. Oikeyama is theoretical, the concept of ice-target impacts is well-supported by studies of craters on icy moons in our solar system, such as Europa and Triton.

Consequently, Mount Oikeyama represents a compelling candidate for Japan's first identified impact crater, offering a window into a powerful cosmic event that shaped the early geological history of the region. The multidisciplinary evidence, including its distinct morphology and the presence of shocked quartz, strongly supports an extraterrestrial origin. The intriguing scenario of an impact during the Last Glacial Maximum, striking an ice-

rich target, adds another layer of complexity to its formation, potentially influencing its original morphology and subsequent preservation. Further detailed research, including high-resolution geological mapping, advanced geophysical imaging, and precise dating of impact-related materials, will be crucial to definitively confirm Mt. Oikeyama's impact origin and fully understand the environmental consequences of such an event in glacial Japan.

References

Melosh, HJ. (1989). Impact Cratering: A Geologic Process. Oxford University Press.

Okumura, T., Gucsik, A., Muto, T., Kayama, M., Sano, S., & Hasegawa, M. (2012). Shock metamorphic features of quartz in rocks from Mt. Oikeyama, Central Japan: Evidence for an impact event. Lunar and Planetary Science Conference, 43, 1904.

Ono, Y. (1990). Glacial and periglacial geomorphology in Japan: Present status and future problems. Geographical Reports of Tokyo Metropolitan University, 25, 1–32.

Sakamoto, M., Gucsik, A., Nishido, H., Ninagawa, K., Okumura, T., & Toyoda, S. (2010). MicroRaman spectroscopy of anomalous planar microstructures in quartz from Mt. Oikeyama: Discovery of a probable impact crater in Japan. Meteoritics & Planetary Science, 45(1), 32–42.

Fizzed troilite in a mesosiderite Asuka881154

Naoji Sugiura and Tomoko Arai Chiba Institute of Technology

Mesosiderites have been metamorphosed after the accretion of metal, and shock heating is often proposed as a possible heat source. However, petrographic studies [e.g.1] show that evidence for shock is not found in most mesosiderites. Here we present petrographic features of troilite in a mesosiderite Asuka881154 that suggest shock heating.

We observed a polished section with SEM and found a texture that may be called "fizzed" troilite. It is unfortunate that this term is loosely defined in literature. Here, the fizzed sulfide is defined by Fig.1a and 1b. (Grey is iron sulfide, small dark (elongated and/or spherical) areas are vesicles and bright ones are metal.) In Fig.1a, the black area around the FeS is silicate. In Fig.1b, small irregular metal grains are seen in FeS but there are no vesicles. There are transitional cases between 1a and 1b where small amounts of vesicles coexist with abundant small metal grains.

Fizzed troilite similar to Fig.1b was reported in [2], but as far as we know the texture shown in Fig.1a is the first report.

There may be many possible explanations of the fizzed troilite shown in Fig.1. Here we give our favorite scenario. A prerequisite is quick heating (presumably by shock). The vesicles were produced by evaporation of S_2 from the FeS. This results in excess Fe in FeS that is seen as small metal grains. In the case of Fig.1a, this occurred below the melting T of FeS (or for a very short time above the melting point). Fizzed FeS like Fig,1a and Fig.1b exist next to each other. FeS in Fig.1b must have been similar to that in Fig.1a initially. But FeS in Fig.1b was heated to higher temperatures (above the melting T of FeS) for a longer time. This resulted in loss of the S_2 gas from the vesicles and the vesicles were eliminated. At this high temperature, metal grains grew larger by coalescence. The result would look like Fig.1b.

One may ask why the texture shown in Fig. 1a has not been reported (at least not widely known) for chondrites for which presence of shock melts (both silicates and metal) is well known [4]. If our scenario is correct, the vesicles contained S₂ gas. It was kept in the vesicles by the strength of the FeS mineral and materials around it. In the case of mesosiderites, metal grains (that are interconnected) provide the strength. In the case of chondrites, which are porous and contain less metal grains, the material strength is low. Then, the S₂ gas in the vesicles could easily explode, disintegrating the FeS grains. Therefore, the texture shown in Fig.1a is unlikely to be observed in chondrites.

We are fairly confident that the fizzed troilite shown in Fig.1 was produced by shock heating. But this should be confirmed by impact experiments on FeS.

References

[1] Haack+, GCA60(1996)2609-2619. [2] Li+, JGR.P., 129(2024)2023JE008124. [3] Moreau+, PEPI, 282(2018)25-38. [4] Tomkins+, GCA, 100(2013)41-59.

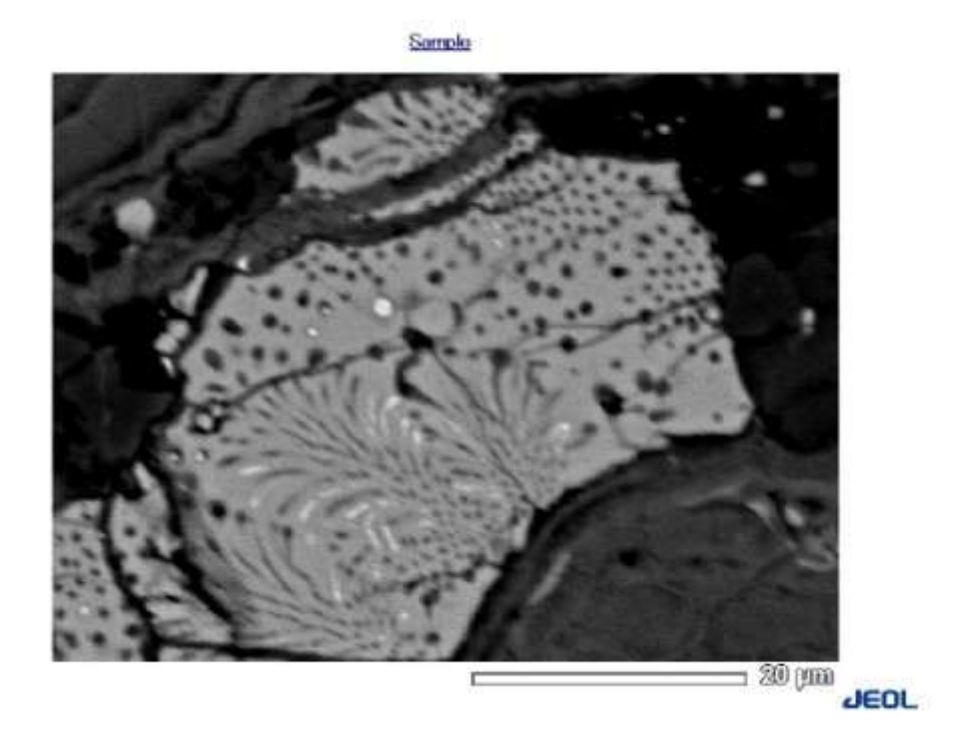


Fig.1a

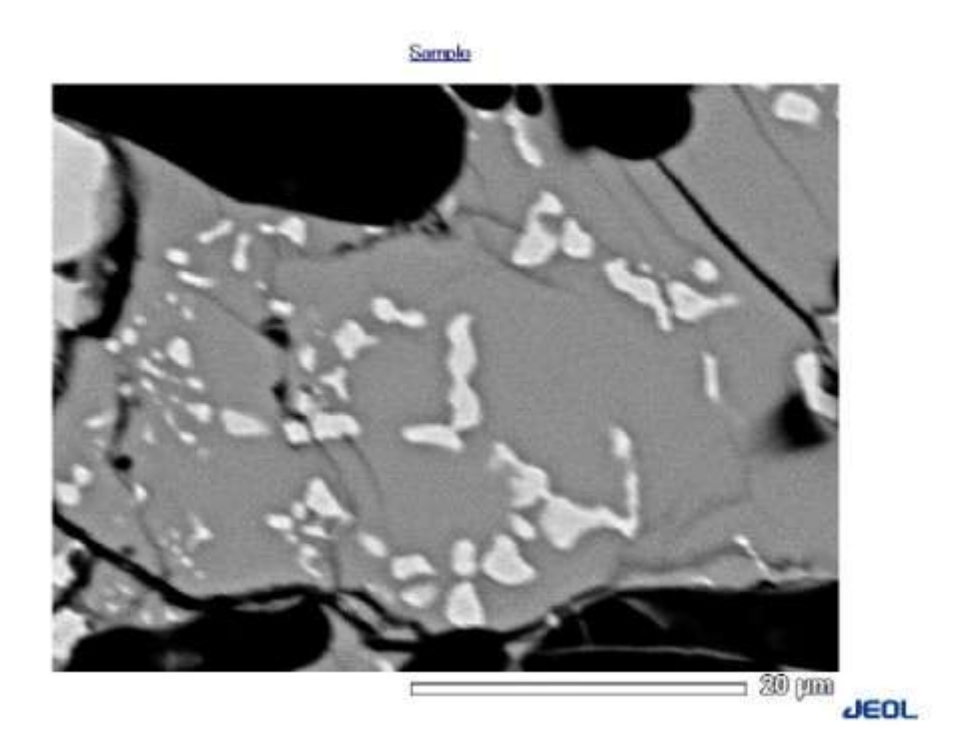


Fig.1b

Assessing HED affinities in achondrites: A comparison of Asuka-881394 and Al Bir Lahlou 001

B. G. Rider-Stokes¹, <u>A. Y. C. Wong¹</u>, A. Yamaguchi², S. L. Jackson¹, R. C. Greenwood¹, M. M. Grady¹, M. Anand¹

School of Physical Sciences, The Open University, Milton Keynes, MK7 6AA, UK.

National Institute of Polar Research, 10-3 Midori-cho, Tachikawa, Tokyo 190-8518, Japan.

Introduction: Howardite-Eucrite-Diogenite (HED) meteorites are believed to have originated from the asteroid (4) Vesta [1]. However, several HED-like meteorites have features that distinguish them from other HEDs, and it has been suggested that they may represent other Vesta-like bodies in the early Solar System [2]. Asuka(A)-881394 is an example of one such anomalous HED-like meteorite, previously classified as a cumulate eucrite based on its petrography and mineralogy [3]. The sample has an anomalous oxygen isotope composition ($\Delta^{17}O=-0.122\%$), which lies more than 15 σ from the eucrite fractionation line (EFL: $\Delta^{17}O=-0.240\pm0.021\%$ (3 σ)) [4,5]. It is also unique among other HEDs due to the plagioclase present in this sample being unusually calcic [6]. In this study, we compare A-881394 with Al Bir Lahlou 001 (ABL 001), an ungrouped achondrite with strong affinities to the HED meteorites [7]. We examine both samples and report on their geochemistry, UV-Vis-NIR reflectance spectra, and their oxygen isotopic compositions.

Sample and methods: Multiple fragments of ABL 001 were donated by Jared Collins. A small fragment was embedded in epoxy resin, polished, and coated with carbon (5 nm). The polished mount was subsequently investigated using a Zeiss Crossbeam 550 SEM at The Open University (OU), UK, to obtain backscatter electron (BSE) and energy dispersive spectroscopy (EDS) maps. Chemical compositions were obtained using an electron probe microanalyzer (EPMA: CAMECA SX100) at the OU. A fine-grained fraction from A-881394 (0.3g) was obtained from the NIPR. Its chemical composition was taken solely from literature data [1,6]; further measurements are planned at NIPR. For each sample, a small amount of material (~0.1g) was crushed by hand using an agate mortar and pestle to produce a homogenised powder (with grain sizes of ~50 μm). Subsequently, the UV-Vis-NIR spectra of both samples were measured using a JASCO MSV-5700 UV-Vis-NIR microspectrophotometer (MSP) at the OU, following established procedures [8]. Oxygen isotope analyses were obtained by laser fluorination at the OU, following established procedures [5,9].

Results and discussion: A-881394 has a coarse-grained granular texture, consisting of pyroxene and interstitial plagioclase [3]. The chemical composition of pyroxenes present in A-881394 is similar to that of the HED suite (Fig. 1a), providing compelling evidence that this sample is closely related to HEDs. However, the plagioclase in A-881394 is extremely calcic. Chemistry data from the literature [6] places the anorthite content between 97 and 98.9, which is resolvable from other HEDs (Fig. 1b). ABL 001 is an unbrecciated cumulate, consisting of near equal amounts of orthopyroxene and poikilitic plagioclase. Its oxygen isotopic composition plots within 3σ of the EFL (Δ¹¹O=−0.242, −0.256, −0.278‰) (Fig. 1d), and the chemical compositions of its pyroxenes are consistent with those of the HED suite (Fig. 1a, b), both strong indicators that this sample is at least closely related to, if not a part of, the HED suite. However, ABL 001 notably deviates from HED ranges in the anorthite content of its plagioclase, and Cr vs Al ratio in pyroxene. Reminiscent of A-881394, the plagioclase in ABL 001 is highly calcic, and its anorthite content is resolvable from other HEDs (Fig. 1b). Furthermore, the Cr vs Al ratio of pyroxene in ABL 001, although falling broadly on the same trendline as other HEDs, is also anomalous (Fig. 1c). A-881394 shows a similar trend, but its deviation from the HED range is less significant. Although the origins of the unusual chemical features mentioned are still unclear, we suggest that it may result from deviations from typical HED igneous evolution [7]. The close similarity between ABL 001 and A-881394 in these two features may indicate that they had both undergone similar processes.

The UV-Vis-NIR spectra of both samples are also evaluated, using band structure analysis methods outlined in [8]. The spectrum of ABL 001 is typical of V-type asteroids [10], and in particular, is a close match to the spectrum of (4) Vesta. This supports the idea that ABL 001 likely originates from the same parent body as other HEDs. A-881394 also shows a typical V-type spectrum, with several V-type asteroids being identified as strong matches. The band I and II features, which are thought to be related to pyroxene, in A-881394 and ABL 001 are similar, but not identical. Notably, the band centre (BIIc) and depth (BIId) of the band II feature of A-881394 is shifted slightly to longward and shallower in comparison to ABL 001. This is most likely attributable to the pyroxene chemistry present in the sample [11]. For example, the higher Ca content in the pyroxene present in A-881394 may be responsible for this shift. Furthermore, although spectral analysis alone cannot unambiguously identify the parent body of a meteorite, this similarity with ABL 001 and V-type asteroids adds weight to the argument that A-881394 originates from a V-type asteroid, which is likely to have undergone differentiation and igneous evolution processes

similar to (4) Vesta itself. However, it must be noted that the anomalous oxygen isotopic composition of A-881394 contradicts the argument that (4) Vesta is its parent body and does not support a relationship to ABL 001.

Summary: The ungrouped achondrite ABL 001 exhibits a number of similarities to anomalous eucrite A-881394, many of which are not shared by the main HED suite. However, based on existing information, it is not clear whether the two are genetically related to each other. While (4) Vesta is the most likely parent body for ABL 001, the parent body of A-881394 is still undetermined. UV-Vis-NIR spectra analysis suggests several V-type asteroids as possible parent bodies from which A-881394 might be derived, and these also show a high degree of similarity to ABL 001. We therefore propose that A-881394 and ABL 001 were the products of parent bodies that experienced closely similar differentiation histories. This suggests that other Vestalike differentiated asteroids existed in the early Solar System but have since been disrupted. Further work on A-881394 is needed to better understand its similarities and differences with the HED meteorites, the origins of its unusual geochemical and isotopic features, and the nature of its relationship to other anomalous HED-like achondrites.

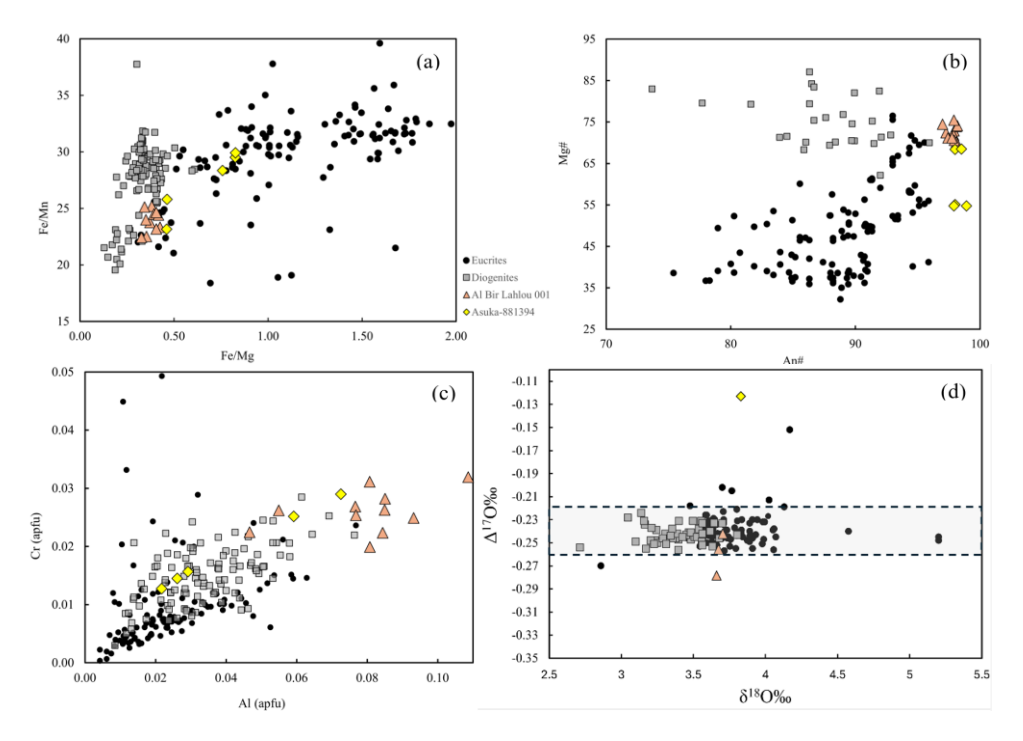


Figure 1. Mineral compositions and oxygen isotopic compositions of ABL 001 and A-881394, compared to other HEDs. The shaded region represents 3σ of EFL. Data for HEDs from [1,4,5]; data for A-881394 from [1,4,5,6].

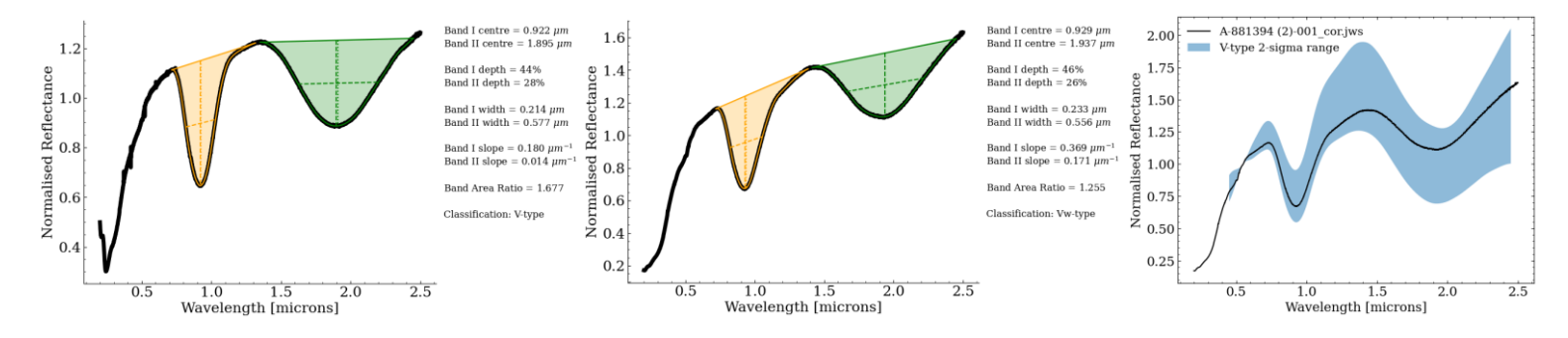


Figure 2. Comparison of spectra of ABL 001 (left), A-881394 (middle), and V-types (right). Note the difference in the Band II centre (BIIc).

References: [1] Mittlefehldt, D.W. (2015). Geochemistry, 75(2), pp.155–183. [2] Burbine, T.H. et al. (2024). MAPS, 59(4). [3] Takeda, H. et al. (1997). Antarctic Meteorite Research, 10, pp.401–413. [4] Scott, E. et al. (2009). Geochim. Cosmochim. Acta, 73(19), pp.5835–5853. [5] Greenwood, R.C. et al. (2017). Geochemistry, 77(1), pp.1–43. [6] Nyquist, L.E. et al. (2003). Earth Planet. Sci. Lett., 214(1-2), pp.11–25. [7] Rider-Stokes, B.G. et al. (Under Review). Icarus. [8] Rider-Stokes, B.G. et al. (2025). Icarus, 432, p.116506. [9] Miller, M.F. (2002). Geochim. Cosmochim. Acta, 66(11), pp.1881–1889. [10] DeMeo, F.E. et al. (2009). Icarus, 202, pp.160–180. [11] Klima, R.L. et al. (2011). MAPS, 46(3), pp. 379-395.

Relationship between shock history and radiometric dating of Martian meteorite

<u>Hisanori Higuchi</u>¹, Masaaki Miyahara¹, Takeshi Sakai², Naotaka Tomioka³, Akira Yamaguchi⁴ *Hiroshima Univ.*, ²Geodynamics Research Center, Ehime Univ., ³JAMSTEC, ⁴NIPR

Martian meteorites are important samples for understanding the evolutionary history of Mars. Radiometric ages of minerals in these meteorites provide key constraints on the timing of igneous activity on Mars. Accordingly, various Martian meteorites have been dated to determine their formation ages. Among them, shergottites—the largest group of Martian meteorites—exhibit remarkably young radiometric ages. Whether these ages reflect the timing of magma crystallization or that of the impact event responsible for ejecting the rocks from Mars has been a subject of ongoing debate.

Niihara et al. (2012) conducted shock-recovery experiments on basalt at pressures up to 57 GPa and reported no significant disturbance to the U–Pb isotopic composition of baddeleyite (ZrO₂). In contrast, Darling et al. (2016) reported that baddeleyite in the basaltic shergottite Northwest Africa (NWA) 5298 had experienced varying degrees of shock metamorphism, with up to ~80% radiogenic Pb loss. They derived a crystallization age of 175 ± 30 Ma from the least-altered grains and a minimum age of the impact event of 22 ± 2 Ma from the most-altered grains. Significant U–Pb isotopic disturbance in baddeleyite has, to date, only been reported for NWA 5298, making it a uniquely valuable sample for examining the relationship between radiometric ages and shock metamorphism in meteorites.

However, the study by Darling et al. (2016) focused primarily on the shock metamorphism of baddeleyite and did not provide detailed estimates of the shock temperature and pressure. In this study, we investigated the shock-induced melt textures and the occurrence of high-pressure minerals in NWA 5298 to estimate shock temperatures and pressures. We then discussed whether such conditions could disturb the U–Pb isotopic system in baddeleyite and the temperature–pressure thresholds required for such disturbance.

Evidence of the shock metamorphism in NWA 5298 includes cracks in clinopyroxene and extensive melting and vesiculation of plagioclase. Melt pockets are distributed throughout the sample and are characterized by quenched textures with tabular crystals of plagioclase and clinopyroxene. These melt pockets also contain silica, and Raman spectroscopy identified coexisting silica glass, coesite, and quartz. Symplectite consisting of fayalitic olivine, silica, and clinopyroxene occurs adjacent to the melt pocket. The silica phase is present as silica glass. Electron diffraction analysis revealed dense stacking faults oriented along the (001) plane of the fayalitic olivine.

From these observations, we estimate that NWA 5298 experienced shock temperatures of at least 1000 °C, locally exceeding 1225 °C, as suggested by the melting of most plagioclase and localized melting of clinopyroxene (Mikouchi and McKay, 2006; Lindsley and Glotch, 2019). The presence of stacking faults along the (001) plane of the fayalite olivine requires pressures ≥39.5 GPa, implying that NWA 5298 was subjected to shock pressures of at least this magnitude (Takenouchi et al., 2019). These estimates may exceed the temperature–pressure conditions reported by Niihara et al. (2012) for basalt in shock-recovery experiments, suggesting that disturbance of the U−Pb system in baddeleyite could occur. Moreover, the duration of the high-temperature state is likely a critical factor in causing such disturbance. Therefore, investigating the cooling of post-shock melt pockets can provide more constraints on the temperature–pressure conditions affecting the U−Pb system in baddeleyite. These insights will ultimately contribute to advancing our understanding of the evolutionary history of Mars.

References

- Niihara T., et al. (2012) U–Pb isotopic systematics of shock-loaded and annealed baddeleyite: Implications for crystallization ages of Martian meteorite shergottites. Earth and Planetary Science Letters 341-344 (2012) 195–210.
- Darling, J. R., et al. (2016) Variable microstructural response of baddeleyite to shock metamorphism in young basaltic shergottite NWA 5298 and improved U–Pb dating of Solar System events. Earth and Planetary Science Letters 444 (2016) 1–12.
- Mikouchi and McKay (2006) Shock Metamorphism of the Dhofar 378 Basaltic Shergottite. 30th Symposium on Antarctic Meteorites, Tokyo.

- Lindsley, D. H., Nekvasil, H., & Glotch, T. D. (2019). Synthesis of pigeonites for spectroscopic studies. American Mineralogist, 104(3), 615–618.
- Takenouchi A., et al.(2019) Fine-structures of planar deformation features in shocked olivine: A comparison between Martian meteorites and experimentally shocked basalts as an indicator for shock pressure. Meteoritics & Planetary Science 54, Nr 9, 1990–2005 (2019) doi: 10.1111/maps.13367.

Planet Formation: What We Can Learn from the 3D Modeling of Chondrules

<u>József Vanyó</u> and Arnold Gucsik Eszterházy Károly Catholic University, Eger, Hungary

Chondrules, the millimeter-sized, spherical igneous rocks found in chondritic meteorites, are fundamental building blocks of planets. They represent some of the earliest solid materials to form in the solar system, making their study crucial for understanding the processes that transformed a swirling disk of gas and dust into the planets we see today. While two-dimensional (2D) analysis of these objects has provided invaluable insights, the true power of understanding their formation lies in three-dimensional (3D) modeling. By reconstructing chondrules in their full volumetric complexity, we can gain new insights into the mechanisms of their formation, their evolutionary history, and the conditions of the early solar nebula.

The formation of chondrules is a central mystery in cosmochemistry. The dominant theory posits that they formed from melted dust aggregates in the protoplanetary disk, but the exact heating mechanism remains a subject of intense debate. Proposed models include shock waves from stellar outflows, lightning discharges, or gravitational instabilities within the disk. 2D studies of chondrule cross-sections have revealed important clues about their mineralogy and texture, such as the presence of porphyritic or barred olivine textures. However, these slices can misrepresent the overall shape and internal structure of the chondrule. For instance, a 2D cross-section might show a small, fractured chondrule, but a 3D model could reveal it to be part of a larger, originally spherical object that was broken after its formation. This level of detail is critical for distinguishing between a primary, small chondrule and a fragment of a larger one, which has significant implications for understanding the size distribution of these early solar system components.

3D modeling, often achieved through X-ray computed micro-tomography (muCT), provides a complete volumetric dataset. This approach allows researchers to not only visualize the entire chondrule but also to analyze its internal components and their spatial relationships without physically destroying the sample. For example, by segmenting and isolating different mineral phases (e.g., olivine, pyroxene, and metallic inclusions) in a 3D model, we can precisely quantify their volumes, surface areas, and connectivity. This is particularly valuable for studying the distribution of metallic veins within a chondrule. Are they truly isolated spheres, or are they part of a complex, interconnected network? A 2D slice might show multiple isolated metal grains, but a 3D model could reveal them to be part of a single, continuous, and complex inclusion. Such detailed analysis can constrain the cooling rates and the redox conditions during the chondrule's formation, offering crucial tests for various formation models.

Furthermore, 3D modeling offers a more accurate method for measuring the size and shape of chondrules. Traditional 2D methods, which rely on measuring a circle's diameter in a random cross-section, often underestimate the true size of the spherical chondrule. This systematic underestimation can skew the chondrule size distribution data, which is a key parameter for many formation models. By calculating the true volume of a chondrule from its 3D model and then determining its equivalent spherical diameter, we can generate a more robust and accurate size distribution. A corrected size distribution could help validate or refute formation theories, such as models proposing that chondrule size is determined by the size of the initial dust aggregates or the strength of a shock wave.

In conclusion, the 3D modeling of chondrules represents a significant leap forward in understanding the fundamental processes of planet formation. It surpasses the limitations of 2D cross-sections to offer a comprehensive, non-destructive view of these ancient objects. The ability to accurately measure true size distributions, quantify the spatial relationships of internal components, and reconstruct a chondrule's complete history offers unprecedented opportunities to test and refine our theories about the early solar nebula. As 3D imaging technology becomes more accessible and sophisticated, the insights gained from this approach will be instrumental in unlocking the remaining mysteries of how planets came to be.

Meteoritic and terrestrial chromium abundances. Implications for the heavy element budget of terrestrial planetary cores.

P. Futó¹, A. Gucsik²

¹University of Debrecen, Cosmochemistry Research Group, Department of Mineralogy and Geology, Debrecen, Egyetem tér 1.

H-4032, Hungary (peter.futopf@gmail.com)

Department of Physics, Eszterházy Károly Catholic University, H-3300, Eszterházy tér 1, Hungary

(E-mail: sopronianglicus@gmail.com).

Chromium is present as a minor element in meteorites. It is an indicator of physical and chemical conditions of meteorite formation. For instance, the rare siderophile chromium is derived from primitive condensation processes (Bunch and Olsen 1975). Meteoritic Cr-minerals with an average of 3 elements per species are mostly sulphides, posphides and nitrides (Liu et al. 2017). Chromium minerals often occur in the structure of spinel group in c-chondrites. These spinel group Cr-minerals are chromite (Fe²⁺Cr₂O₄) and the magnesiochromite ((MgCr₂O₄).

A comparative analysis have been performed for chromium budgets of iron meteorites, C-chondrites, bulk-Earth and Earth's core to obtain results, which may helps to understand the heavy element compositions of the terrestrial planetary cores in the Solar System. Assuming the abundances of heavy elements in Earth and other terrestrial planets are similar to the examined meteoritic compositions, we compare Cr-abundances in the different planetary materials having implications for the Cr-budgets in the metallic cores of the Solar System terrestrial planets. Published values of chromium budget of bulk Earth, Earth's core, C-chondrites and IAB iron meteorites are listed in Table 1.

	IAB iron (Canyon Diablo)	CI chondrite	Bulk Earth	Earth's core
Chromium content	26 ppm ¹	0.265 wt% ²	0.44^2 0.429^3	0.8 wt% ² 0.779 wt% ³

Table 1. Chromium abundance data for meteoritic and planetary materials. ¹Wasson and Kallemeyn 2002; ² McDonough and Sun 1995; ³ Allégre et al. 1995

The chemcial composition of the metallic mineral components in the carbonaceous chondrites can be similar to the iron-bearing meteorites (Futó and Gucsik 2021). The relative abundance of Fe, Ni, Co, Mn, Cr and P in the metallic cores of terrestrial planetary bodies can also be similar to the abundances of carbonaceous chondrites. Thus, the chromium composition of C-chondrites implies on the heavy element composition of the Fe-dominated metallic cores of chondrite parent asteroids and the Solar terrestrial planets. Based on cosmochemical and geochemical considerations and the relevant CI-chondritic abundances of the inner Solar-System planets, chromium is suggested to be the one of the most abundant heavy elements (Fe,Ni,Co,Mn,Cr, P) in the Earth's core.

References

Allégre CJ, Poirier J.-P, Humler E, Hofmann AV. The chemical composition of the Earth. Earth and Planetary Science Letters, 134, 515-526, 1995.

Bunch TE., Olsen E.: Distribution and significance of chromium in meteorites. Geochimica et Cosmochimica Acta. 39, 911-922, 1975.

Futó P, Gucsik A. Chemical analyses of Fe-rich chondrule phases in Kaba (CV3) carbonaceous-chondrite. Implications on the bulk elemental composition of terrestrial planetary cores. The 12th Symposium on Polar Science. OAp4. 2021.

Liu C, Hystad G, Golden JJ, Hummer DR, Downs RT, Morrison SM, Ralph JP; Hazen RM. Chromium mineral ecology. American Mineralogist 102, 612-619, 2017.

McDonough WF, Sun S. The composition of the Earth. Chemical Geology, 120, 223-253, 1995.

Wasson JT, Kallemeyn GW. The IAB iron-meteorite complex: A group, five subgroups, numerous grouplets, closely related, mainly formed by crystal segregation in rapidly cooling melts. Geochimica et Cosmochimica Acta. 66, 2445-2473, 2002.

The interstellar alloy: future perspectives

<u>Arnold Gucsik</u> Eszterházy Károly Catholic University, Eger, Hungary

This is a fascinating topic that spans Astrophysics, Chemistry, and Planetary Science. However, it's important to clarify that the existence of naturally occurring interstellar alloys, in the form of macroscopic fragments, has not been scientifically confirmed or discovered. While we have evidence of interstellar dust and some specific elements, the concept of a complex alloy forming in interstellar space and then being found on Earth is, for now, a subject of theoretical speculation rather than fact. Therefore, this abstract is based on what is scientifically plausible and confirmed, discussing the interstellar materials we have found and their potential link to interstellar objects like 'Oumuamua and 2I/Borisov, for instance.

The notion of an "interstellar alloy" evokes a sense of advanced, extraterrestrial metallurgy, but in reality, the interstellar medium (ISM) is a harsh environment where atoms and simple molecules are the norm. The interstellar dust that pervades our galaxy consists primarily of tiny, sub-micron-sized particles of silicates and carbonaceous materials. These stardust particles are formed in the cool, expanding atmospheres of evolved stars, such as red giants and supernovae, and are then ejected into the ISM. They serve as the building blocks for new stars and planets. While some metallic elements like iron (Fe), nickel (Ni), and magnesium (Mg) are present, they are typically found as single atoms or within simple mineral grains, such as iron-magnesium silicates, not as complex, macroscopic alloys.

The discovery of the first two confirmed interstellar objects, 1I/Oumuamua and 2I/Borisov, marked a turning point in our understanding of interstellar matter. Oumuamua, a highly elongated object with an extremely eccentric orbit, exhibited no cometary activity, leading to speculation about its composition. One intriguing hypothesis proposed that its tumbling motion and high density could be explained if it were a solid fragment of a tidally disrupted planetesimal composed of a metallic alloy (Moro-Martín, 2019). While this remains speculative, it opened the door to considering that interstellar space might contain fragments of a more complex nature than simple dust grains.

In contrast, 2I/Borisov was undeniably a comet, displaying a clear cometary coma and a tail. Its composition, based on spectroscopic analysis, showed that it was rich in carbon monoxide (CO) and cyanide (CN), similar to some comets in our own solar system but with a higher-than-average CO content. This indicates that while it formed in another star system, its basic chemistry and composition were consistent with what we know about comets.

The third interstellar object candidate, 3I/ATLAS, was a comet that disintegrated as it approached the Sun, preventing detailed analysis. While the search for these objects continues, their study is our best chance of directly sampling the building blocks of other star systems.

While we haven't found a macroscopic interstellar alloy, we have found microscopic interstellar grains embedded within certain meteorites, particularly the most primitive ones. These grains are the only solid, pre-solar materials we can physically hold and analyze. They are identified by their anomalous isotopic compositions, which differ from anything formed within our solar system. The most common types of these grains are:

- Silicon Carbide (SiC): Often referred to as "stardust," SiC grains are formed in the carbon-rich atmospheres of AGB (Asymptotic Giant Branch) stars. They are identified by their highly unusual isotopic ratios of carbon and silicon.
- Nanodiamonds: These tiny crystals of carbon are thought to have formed in supernovae explosions.
- Graphite Grains: Another form of carbon, these grains show isotopic anomalies that link them to stellar origins.

The study of these grains provides invaluable insights into the nuclear processes of stars and the conditions in the interstellar medium before the formation of our solar system. The presence of metallic elements like iron within these grains suggests that if a complex alloy were to form, it would likely be on a tiny scale, incorporated

within these dust particles. These conditions are generally not met in the diffuse ISM. Instead, they are found in the immediate vicinity of a star's formation, within protoplanetary disks, or in highly energetic events like supernovae. It is far more plausible that an interstellar object like 'Oumuamua, if it were metallic, was a fragment of a planetesimal that formed and was then ejected from its home star system, rather than an alloy that spontaneously formed in interstellar space.

In conclusion, while the discovery of an "interstellar alloy" would be a monumental finding, the current scientific evidence suggests that such complex materials are not a common feature of the interstellar medium. Our current understanding points to the presence of simple elements and microscopic mineral grains (stardust) that are the building blocks of planets. Interstellar objects like 'Oumuamua and 2I/Borisov provide us with our first direct look at the composition of other star systems, and while one may have been a metallic fragment, it was likely formed in a protoplanetary disk, not in interstellar space. The true interstellar materials we have in hand are the presolar grains found in meteorites, which are our windows into the stellar nurseries of our galaxy. Further study of new interstellar objects and the hunt for more presolar grains will continue to refine our knowledge of the material composition of the universe beyond our Solar System.

Identification and Distribution of Evaporites in Antarctic Meteorites

<u>Aiko Nakato</u>¹, Naoya Imae¹, and Akira Yamaguchi¹ *National Institute of Polar Research*

Introduction:

It has been reported that many meteorites recovered in Antarctica contain evaporites, which are secondary minerals formed on Earth, on their surfaces or within fractures [e.g., 1-3]. These phases mainly consist of Mg- and Ca-bearing carbonates (e.g., nesquehonite Mg(HCO₃)(OH)·2H₂O, hydromagnesite Mg₅(CO₃)₄(OH)₂ · 4H₂O) and sulfates (e.g., starkeyite MgSO₄·4H₂O, gypsum CaSO₄·0.5H₂O) [e.g., 1-3], and coexist with the primary minerals of the interior rock. In particular, carbonates have the risk of being interpreted as aqueous alteration products on the parent body (e.g., the abundant terrestrial dolomite in Yamato (Y) 980115 (CI/CY) [4]), which could affect classification and the interpretation of their evolution history. This study aims to clarify the constituent minerals in both the original rock (interior) and surface inclusions, and to establish criteria for distinguishing evaporites from primary minerals. The identification of evaporites will contribute to the evaluation of the storage environment of meteorite samples, appropriate sample allocation according to proposal requirements, and the development of curatorial work that accounts for material changes during long-term storage.

Samples and Methods:

Samples were prepared from two Antarctic ordinary chondrites, Y-74371 (H4) and Belgica (B) 9826 (L6). For each meteorite, interior and evaporite samples were separated. Surface-attached evaporites were carefully scraped off using a W-needle under a stereomicroscope and then recovered. The interior samples, consisting of rock chips without fusion crust or evaporite, were ground into powder using an agate mortar. For Y-74371, evaporite was attached mainly to the fusion crust portion. Therefore, for comparison, a powder sample was also prepared from the fusion crust portion in the same manner as the interior.

Powder X-ray diffraction (XRD) analysis was performed at the National Institute of Polar Research, Japan, on these five samples (Y-74371 interior, fusion crust, evaporite; B 9826 interior, evaporite). Each sample (\sim 5 mg) was placed to fill a 5 mm diameter, 0.2 mm deep hole in a non-reflective silicon plate and gently pressed with sapphire glass to level the surface. The SmartLab (Rigaku) instrument was used, and the analysis conditions, as described in [5], were as follows: Cu K α with Ni-filter at 40kV and 40 mA; $2\theta = 10-70^{\circ}$; approximately 120 minutes measurement duration for each sample. The data were processed using Rigaku PDXL2 software and ICDD PDF-4/Minerals 2025 database.

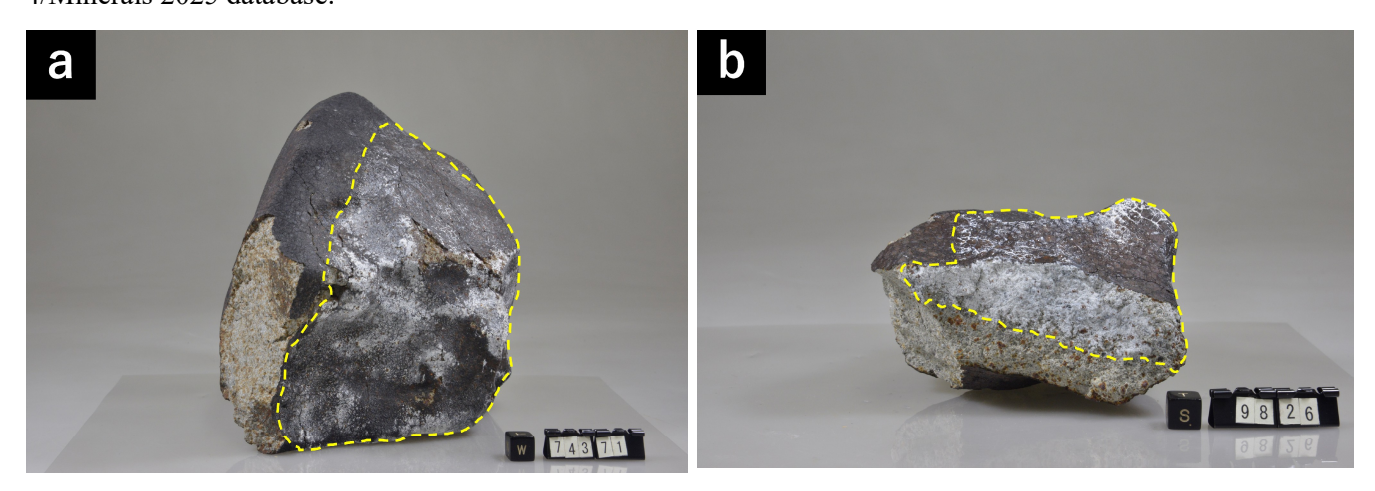


Figure 1. Photographs of ordinary chondrites showing prominent evaporites on their surfaces. Evaporites are observed in the area outlined by the yellow dashed line. Scale: black cube = 1 cm. (a) Yamato-74371, original main mass: 5067.9 g, H4 chondrite. Most of the surface is covered by fusion crust. Evaporite minerals are observed primarily on the fusion-crust areas. (b) Belgica 9826, original main mass: 959.22 g, L6 chondrite. Evaporites are observed on both the fusion crust and the broken surfaces.

Results and Discussion:

The XRD patterns of the interior samples well reflect the host rock mineralogy. The peak positions (2θ) and relative intensities of the olivine/pyroxene reflections indicate that Y-74371 (H4) is relatively Mg-rich, while B-9826 (L6) is relatively Fe-rich. Regarding the difference between the fusion crust and interior of Y-74371, while not completely resolved due to the difficulty of physically separating the samples, the overall XRD patterns are broadly similar, with the fusion crust showing lower relative pyroxene peak intensities. This is consistent with previous studies indicating olivine preferentially crystallizes early from melt during atmospheric entry [6].

For evaporites, nesquehonite was dominant in both Y-74371 and B 9826, with minor detections of starkeyite and hydromagnesite. This trend is consistent with previous studies showing Mg carbonate predominance and minor sulfate content in ordinary chondrites [3, 7]. Although differing in origin from evaporites, akaganeite and jarosite, commonly known as rust deposits on Antarctic meteorite surfaces [8], were not detected by XRD in these meteorites.

We plan to verify the systematic difference in Mg-sulfate dominance by XRD experiments on carbonaceous chondrites Y-793595 (CM2) and Y 980115 (CI/CY) and confirm the occurrence and chemical composition using SEM-EDS.

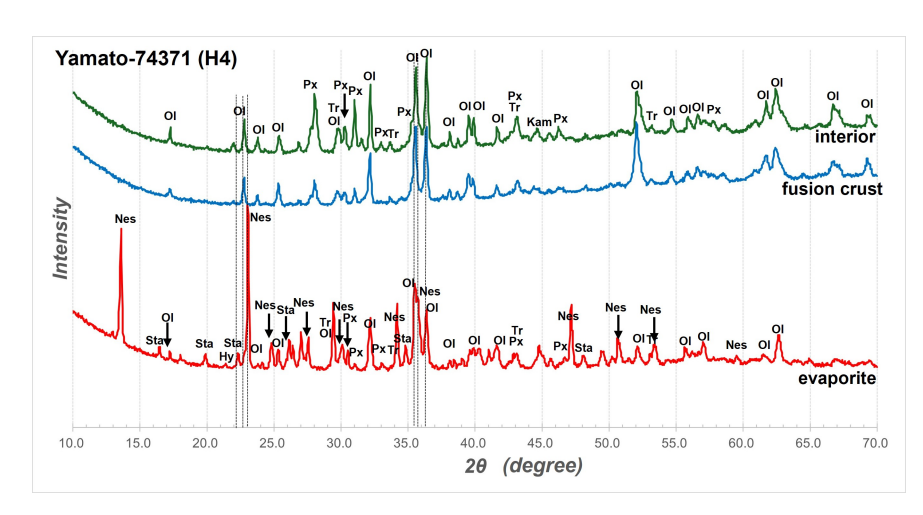


Figure 2. X-ray diffraction patterns of Y-74371 (H4). Abbreviations; Ol, forsterite (Mg_{1.8}Fe_{0.2})SiO₄; Px, enstatite (Ca_{0.069}Mg_{1.490}Fe_{0.077})Si₂O₆; Tr, troilite; Kam, kamacite; Nes, nesquehonite; Sta, starkeyite; Hy, hydromagnesite. The XRD pattern of fusion crust is broadly similar to the interior but with slightly lower pyroxene peak intensities. Evaporite sample is dominated by nesquehonite, with minor starkeyite and hydromagnesite.

References

- [1] Velbel, M.A., Long, D.T., & Gooding, J.L. (1991) Terrestrial weathering of Antarctic stony meteorites: Formation of Mg-carbonate efflorescences on ordinary chondrites. *Geochimica et Cosmochimica Acta* **55**, 67–76. [2] Bland, P.A., Benedix, G.K., & Jull, A.J.T. (2006) Weathering of chondritic meteorites. In: Lauretta, D.S. & McSween, H.Y. Jr. (eds), *Meteorites and the Early Solar System II*. University of Arizona Press, Tucson, pp. 853–867.
- [3] Velbel, M.A. (1988) The distribution and significance of evaporitic weathering products on Antarctic meteorites. *Meteoritics* **23**, 151–159.
- [4] Urashima, S., Tsuchiya, H., Imae, N., Yamaguchi, A., & Yui, H. (2025) Raman spectroscopic analysis of carbonates on a CY-type carbonaceous chondrite Yamato 980115: unexpectedly abundant terrestrial weathering products. *Analytical Sciences* **41**, 689–695.
- [5] Imae, N., Tomioka, N., Uesugi, M., Kimura, M., Yamaguchi, A., Ito, M., et al. (2024) Mineralogical approach on laboratory weathering of uncontaminated Ryugu particles: Comparison with Orgueil and perspective for storage and analysis. Meteoritics & Planetary Science 59, 1705–1722.
- [6] Genge, M.J., & Grady, M.M. (1999) The fusion crusts of stony meteorites: Implications for the atmospheric reprocessing of extraterrestrial materials. *Meteoritics & Planetary Science* **34**, 341–356.
- [7] Yabuki, H., Okada, A., and Shima, M. (1976) Nesquehonite Found on the Yamato 74371 Meteorite. *Scientific Papers of the Institute of Physical and Chemical Research* **70**, 1, 22-29.
- [8] Buchwald, V.F., & Clarke, R.S., Jr. (1989) Corrosion of Fe–Ni alloys by Cl-containing akaganeite (β-FeOOH): The Antarctic case. *American Mineralogist* **74**, 656–667.